Developmental Biology 456 (2019) 86–103

Contents lists available at ScienceDirect

Developmental Biology

journal homepage: www.elsevier.com/locate/developmentalbiology

Functional role of *pax6* during eye and nervous system development in the annelid *Capitella teleta*

Marleen Klann, Elaine C. Seaver *

Whitney Laboratory for Marine Bioscience, University of Florida, 9505 Ocean Shore Blvd, St. Augustine, Fl, 32080, USA

ARTICLE INFO

Keywords:
pax6
Eye
Nervous system
Annelid
Morpholino
Capitella

ABSTRACT

The transcription factor Pax6 is an important regulator of early animal development. Loss of function mutations of *pax6* in a range of animals result in a reduction or complete loss of the eye, a reduction of a subset of neurons, and defects in axon growth. There are no studies focusing on the role of *pax6* during development of any lophotrochozoan representative, however, expression of *pax6* in the developing eye and nervous system in a number of species suggest that *pax6* plays a highly conserved role in eye and nervous system formation. We investigated the functional role of *pax6* during development of the marine annelid *Capitella teleta*. Expression of *pax6* transcripts in *C. teleta* larvae is similar to patterns found in other animals, with distinct subdomains in the brain and ventral nerve cord as well as in the larval and juvenile eye. To perturb *pax6* function, two different splice-blocking morpholinos and a translation-blocking morpholino were used. Larvae resulting from microinjections with either splice-blocking morpholino show a reduction of the *pax6* transcript. Development of both the larval eyes and the central nervous system architecture are highly disrupted following microinjection of each of the three morpholinos. The less severe phenotype observed when only the homeodomain is disrupted suggests that presence of the paired domain is sufficient for partial function of the Pax6 protein. Preliminary downstream target analysis confirms disruption in expression of some components of the retinal gene regulatory network, as well as disruption of genes involved in nervous system development. Results from this study, taken together with studies from other species, reveal an evolutionarily conserved role for *pax6* in eye and neural specification and development.

1. Introduction

Pax genes are a diverse family of transcription factors that function in a range of developmental processes (Mansouri et al., 1996; Noll, 1993), and are mainly characterized by the presence of two DNA binding domains, a paired domain and a paired-type homeodomain; each domain recognizes different downstream target genes (Chi and Epstein, 2002). The Pax6 transcription factor has two conserved roles during animal development. First, it functions early in an eye induction cascade to initiate transcription of numerous genes involved in eye development. In vertebrates, the paired-type homeodomain has been shown to be important for developmental processes of the eye such as lens formation and retinal specification (Ashery-Padan et al., 2000; van Heyningen and Williamson, 2002). Second, Pax6 broadly regulates various other aspects of neurogenesis. For example, the balance between neural progenitor proliferation and differentiation during brain development is controlled by the paired domain (Haubst et al., 2004; Walcher et al., 2013). The importance of Pax6 during these two crucial developmental processes is also evident by identification of numerous target genes, which have been studied mainly in mouse (Holm et al., 2007; Purcell et al., 2005; Sansom et al., 2009; Visel et al., 2007), zebrafish (Coutinho et al., 2011) and fruit fly (Halder et al., 1998; Ostrin et al., 2006). Direct and predicted targets such as *opsin* (Sheng et al., 1997), *eyes absent* (Coutinho et al., 2011; Halder et al., 1998; Purcell et al., 2005), *six1/2* (Halder et al., 1998; Ostrin et al., 2006), *six3/6* (Coutinho et al., 2011; Ostrin et al., 2006; Purcell et al., 2005), and *dachshund* (Coutinho et al., 2011; Purcell et al., 2005) are essential during eye formation. Likewise, target genes such as *neurogenin* (Bel-Vialar et al., 2007; Scardigli et al., 2003), *neuroD* (Coutinho et al., 2011; Holm et al., 2007; Sansom et al., 2009; Visel et al., 2007), *achaete-scute* (Holm et al., 2007; Sansom et al., 2009), *synaptotagmin IV* (Ostrin et al., 2006), and *pax2* (Coutinho et al., 2011; Matsunaga et al., 2000) are indispensable for nervous system development. Moreover, in mouse, fly and *Platynereis dumerilii*, homozygous *pax6* mutants are embryonic lethal (Dobiasovska, 2016), while heterozygous

* Corresponding author.
E-mail address: seaver@whitney.ufl.edu (E.C. Seaver).

https://doi.org/10.1016/j.ydbio.2019.08.011
Received 29 January 2018; Received in revised form 16 August 2019; Accepted 16 August 2019
Available online 21 August 2019

mutants have reduced or no eyes, and show underdeveloped brain structures and neural pathfinding defects (Halder et al., 1998; Hill et al., 1991; Huettl et al., 2016; Nomura et al., 2007).

Although there are numerous studies on the function of *pax6* in ecdysozoans and chordates (Aleen Remez et al., 2017; Ericson et al., 1997; Haubst et al., 2004; Huettl et al., 2016; Nakayama et al., 2015), there is very limited functional data for *pax6* in the third bilaterian superclade, the lophotrochozoans. This species-rich and diverse super phylum is comprised of annelids, mollusks, platyhelminthes, and brachiopods among others. In planarians, it has been shown that *pax6* is required for eye regeneration (Pineda et al., 2002). However, it is currently unknown if *pax6* has a central role in development of the eye and nervous system in this large and diverse animal clade, though expression data for *pax6* in a handful of lophotrochozoan species is consistent with this scenario. While substantial progress has recently been made to develop techniques that alter gene expression, there are still many animals where functional genomic studies are not yet established. To date, only a few representatives within Lophotrochozoa have been shown to be amenable for functional genomic studies, including the annelids *P. dumerilii* (Bannister et al., 2014; Conzelmann et al., 2013) and *Helobdella robusta* (Song et al., 2002), the mollusks, *Tritia obsoleta* (Rabinowitz et al., 2008) and *Crepidula fornicata* (Henry et al., 2010; Perry and Henry, 2015), and the planarians *Dugesia japonica* and *Girardia tigrina* (Pineda et al., 2002). In recent years, the marine annelid *Capitella teleta* has been successfully used for investigations related to evolutionary and developmental processes, and also for regeneration and environmental studies (Amiel et al., 2013; de Jong and Seaver, 2016; Meyer et al., 2010; Meyer et al., 2015; Pechenik et al., 2000; Pechenik et al., 2016; Seaver, 2016; Sur et al., 2017). To further add to the importance of *C. teleta* as a representative annelid, functional genomic studies need to be established. The ability to alter gene expression is of critical importance since this enables the establishment of a direct link between expression of particular genes and their specific functions, and gives insights into the consequences of loss or gain. In the present study, we investigated the role of *pax6* during the development of a lophotrochozoan representative, *Capitella teleta*. Functional data was acquired via microinjections of splice-blocking and translation-blocking antisense morpholinos (MO) into uncleaved embryos of *C. teleta*. Embryos were raised to larval stages and analyzed for phenotypic changes resulting from *pax6* transcript reduction.

2. Materials and methods

2.1. Animal husbandry of C. teleta and Ct-pax6 morpholino injections

A culture of *C. teleta* was kept in the laboratory following previously described methods (Seaver et al., 2005). Metamorphosis was induced by adding mud to competent larvae (Seaver et al., 2005). To obtain uncleaved eggs for morpholino injections, five females and four males were separated for at least two days, and then combined 11 h before checking for presence of fertilized eggs. After dissecting the eggs from the brood tube, the egg membrane was softened by a 25 s incubation with a freshly prepared 1:1 solution of 1M sucrose:0.25M sodium citrate, with at least three subsequent washes in 0.2 μm filtered seawater (FSW). Quartz needles (QF 100-50-10, Sutter Instruments) were pulled on a micropipette puller (P-2000, Sutter Instruments) and used for pressure-injections. The needles were filled with a mixture comprised of the desired concentration of antisense morpholino oligos, nuclease-free water, and a 1:10 dilution of 20 mg/mL red dextran (Texas Red®, Molecular Probes™, dissolved in FSW). Injected and uninjected animals from the same brood were raised in FSW (with 60 μg/ml penicillin and 50 μg/ml streptomycin added) in separate dishes, and compared to determine the health of the brood. A brood was considered healthy if more than 90% of the uninjected animals developed normally. Two different splice-blocking morpholinos (designed by Gene Tools) directed against *C. teleta Ct-pax6* were tested: MO-1 (5′ AAGGGAAGAGGAGAGCCTACCTCTC 3′, Gene Tools) blocks splicing at the second exon-intron boundary and MO-2 (5′ ACTGACAGATTCATTAGTCTTACCT 3′, Gene Tools) blocks splicing at the fourth exon-intron boundary. In addition, a translation-blocking morpholino, MO-trans (5′ AGCCTCCGATCCAACTAGAGCTTCC 3′, Gene Tools), was tested to completely block translation of the entire protein. To detect any potential nonspecific toxicity of the *Ct-pax6* morpholinos, we employed two different control morpholinos: a generic standard control morpholino provided by Gene Tools, control MO (5′ CCTCTTACCTCAGTTACAATTTATA 3′, Gene Tools) and a morpholino related to MO-1 with mismatches at 5 positions, called mismatch MO (5′ AAcGcAAGAcGAGAcCCTAgCTCTC 3', Gene Tools). The sequences of all morpholinos employed in this study were checked for potential off-target binding site in other genes by performing a Blast search against the publicly available *Capitella teleta* genome. All morpholinos were injected into uncleaved eggs, so that the entire embryo was affected by the reduction of *Ct-pax6* expression.

2.2. Fixation, immunohistochemistry and whole mount in situ hybridization of C. teleta larvae and juveniles

Animals were raised to larval stages, and prior to fixation, were relaxed in 1:1 FSW:0.37M $MgCl_2$ for 15 min (see (de Jong and Seaver, 2016) for recovery and pre-treatment of juveniles prior to fixation). *C. teleta* larvae and juveniles were either fixed with 4% PFA in FSW for 30 min at room temperature (antibody labeling) or overnight at 4 °C (whole mount *in situ* hybridization). Samples for antibody labeling were subsequently washed with PBS and processed within 2–3 weeks. Samples for whole mount *in situ* hybridization were washed with PBS, then gradually transferred into 100% methanol and stored at −20 °C for extended periods.

DIG-labeled RNA probes were prepared for *Ct-pax6* (accession number: EY648731.1) (1255 bp) and *Ct-r-opsin1* (accession number: MG225382) (1057 bp) according to standard protocols using the T7 MEGAscript kit (Invitrogen). The colorimetric *in situ* protocol published previously (Seaver and Kaneshige, 2006; Seaver et al., 2001) was followed using a 1 ng/μL DIG-labeled RNA probe with a hybridization step for 72 h at 65 °C. Detection of the DIG-labeled RNA probe was either carried out using NBT/BCIP (Seaver et al., 2001) or fast red following the manufacturer protocol (SigmaFast™ Fast Red TR/Naphthol AS-MX Tablets). The color reaction was stopped after 2 h for both methods of detection.

Antibody labeling followed previously published protocols (Meyer et al., 2015). Primary antibodies and concentrations used were: 1:10 mouse anti-22C10 (Developmental Studies Hybridoma Bank), 1:200 rabbit anti-5HT (Immunostar) and 1:400 mouse anti-acetylated α-tubulin (Sigma). Secondary antibodies and the concentrations used were: 1:500 donkey anti-mouse Alexa 546 (Invitrogen), 1:300 goat anti-rabbit Alexa 488 (Invitrogen) and 1:400 anti-mouse HRP (Jackson Immunoresearch). In *C. teleta*, anti-22C10 specifically labels sensory cells of the eyes (Yamaguchi and Seaver, 2013). Tyramide signal amplification of the 22C10 signal was used occasionally with the following steps. After the immunohistochemistry protocol, samples were washed twice for 10 min in Tyramide buffer (2M NaCl, 0.1M Boric Acid, pH 8.5), and followed with a 10 min incubation in Development Solution (Tyramide buffer, 1:1000 IPBA 20 mg/mL stock diluted in DMF, 1:10000 3% H_2O_2) with 1:1000 Rhodamine-conjugated tyramide (self-made, protocol adapted after (Hopman et al., 1998)). *C. teleta* larvae possess segmental chaetae in the trunk that are highly auto-fluorescent and, based on their distinct morphology and position, are uniquely identifiable. All larvae were counterstained with 1 μg/ml Hoechst 33342 (Life Technologies) for 30 min in PBS, transferred into 70% glycerol/PBS and subsequently mounted onto microscope slides for imaging.

2.3. RT-qPCR

Typically, 150–200 larvae (stage 6) were pooled for one biological replicate. The larvae were put in TRIzol (Invitrogen) and stored at −80 °C until further processing. RNA was extracted from the homogenised samples following a standard phenol/chloroform protocol. Prior to cDNA synthesis (SuperScript® III First-Strand, Invitrogen), the RNA was treated for at least 1 h with DNAse (2 Units, TURBO DNA-free ™, Invitrogen). The RNA input for each cDNA synthesis reaction (total volume of 20 µL) was standardized to 400 ng. Control samples to check for presence of residual genomic DNA contamination were made for each RNA sample by omitting the reverse transcriptase enzyme during the cDNA synthesis reaction (henceforth referred to as "-RT-control"). A Lightcycler 480 Real-time PCR instrument (Roche) was used for RT-qPCR reactions with a SYBR green kit (LightCycler® 480 SYBR Green I Master, Roche). Each RT-qPCR reaction contained the following mix: 5 µL 2x SYBR green mix, 2.5 µL H_2O, 1 µL 5 µM forward primer, 1 µL 5 µM reverse primer, 0.5 µL cDNA. Technical triplicates were run for each individual biological replicate. Each experimental sample is represented by at least 3 biological replicates (a biological replicate is a set of embryos from a single brood). PCR cycling conditions followed standard programs with 40x [10 s 95 °C, 20 s 62 °C, 20 s 72 °C], except for the exon-exon primer pairs (see below) with 40x [20 s 95 °C, 30 s 62 °C, 30 s 72 °C] due to an increased length of the expected fragment. To select a suitable reference gene for calculating relative expression levels, four house-keeping genes were tested: *Ct-CDC5* (*C. teleta cell division cycle 5*), *Ct-RPS9* (*C. teleta ribosomal protein S9*), *Ct-HPRT* (*C. teleta hypoxanthine phosphoribosyl transferase*), and *Ct-EF1* (*C. teleta elongation factor 1*) (Suppl. Fig. 1). *Ct-HPRT* was chosen as an appropriate reference gene for two main reasons. First, since this is a developmental study, it was important that the reference gene shows stable expression across different developmental stages. Five larval stages, stage 4, stage 5, stage 6, stage 7, and stage 7/8 were examined (Suppl. Fig. 1). Since *Ct-CDC5* was found to have higher expression during larval stage 7/8 (yellow curve in Suppl. Fig. 1), it was excluded. Second, the expression levels of *Ct-HPRT* (green curve in Suppl. Fig. 1) are most similar to the expression level of the gene of interest, *Ct-pax6* (blue curve in Suppl. Fig. 1), while *Ct-RPS9* and *Ct-EF1* expression levels are much lower (red and purple curves in Suppl. Fig. 1). Two sets of primers to validate the efficiency of the *Ct-pax6* morpholinos were designed for each of the two splice-blocking MOs. The sequences of all primers used can be found in Suppl. Table 1. The *Ct-pax6* primer sets whose targets are located on exons, F1&R1 and F3&R3, will detect a reduction of the spliced *Ct-pax6* transcript in larvae injected with MO, since the inclusion of the intron will make the qPCR amplicon too long to be synthesized. The *Ct-pax6* primer sets that are targeted to introns, F2&R2 and F4&R4, will detect unspliced *Ct-pax6* transcript only, meaning they will only amplify a product either in cDNA samples which have been modified due to MO activity, or in genomic DNA. cDNA samples used for analysis of potential downstream targets were the same as used for determination of the MO efficiency.

2.4. Statistical analyses

Relative expression ratios were calculated using the method reported in Pfaffl (2001). This method takes into consideration that amplification efficiency between the reference gene and the experimental genes is often not exactly the same, and therefore primer efficiencies for individual genes are incorporated into the formula. Calculation of primer efficiency (E) and other statistical analyses were performed in Microsoft Excel. To calculate the primer efficiency, a standard curve was generated for each primer set for every individual qPCR reaction performed using the following dilutions of cDNA: undiluted, 1:2, 1:4, 1:8, 1:16 and 1:32. The average Ct values of technical triplicates were plotted, and a line of best fit was added to determine the slope. The primer efficiency is $E = 10^{-1/slope}$. The primer efficiency was determined for every individual qPCR experiment and was taken into account when calculating the relative fold change values. Fold change was calculated as

$$R = \frac{E(interest)^{\Delta Ct\ \ interest\ (uninjected-experimental)}}{E(reference)^{\Delta Ct\ \ reference\ (uninjected-experimental)}}$$

Student's *t*-tests were used to determine if different treatment groups showed statistically significant relative fold changes (statistical significance if $p \leq 0.05$). A two-tailed Student's *t*-test was used to determine if there were statistically significant differences in the *Ct-pax6* transcripts of larvae resulting from control MO injections compared to larvae resulting from uninjected embryos. A one-tailed Student's *t*-test was used to determine if there were statistically significant differences in the relative *Ct-pax6* transcript levels from larvae resulting from *Ct-pax6* MO injections compared to larvae resulting from control MO injections. For analysis of downstream target genes, a one-tailed Student's t-test was used to calculate *p* values because the morphological phenotypic changes negatively affected the formation of the nervous system, eye and segment boundary. RT-qPCR results for one of the four biological replicates for the downstream target analysis varied quite a lot from the remaining three biological replicates. However, since multiple technical replicates of this particular biological replicate were consistent, this appears to represent biological variation. Therefore, all four biological replicates were pooled to calculate the final fold change values.

2.5. Documentation and analysis

Colorimetric *in situ* hybridization signals were documented with a digital Spot FLEX camera (Diagnostic Instruments) connected to an Axioskop2 mot plus compound microscope (Zeiss). Fluorescent labeling, including fast red *in situ* hybridization signal, antibody and nuclear staining, was documented with a Zeiss confocal laser scanning microscope 710 (Zeiss) using the ZEN 2011 software. To combine/render image stacks of individual larvae or juveniles taken with the Axioskop2 compound microscope, the software Helicon Focus (d-Studio Ltd.) was used (method B, radium 50 and smoothing 1–7). Confocal image stacks were analyzed and imaged with either the 3D-reconstruction software IMARIS (Bitplane AG) or Fiji (ImageJ; National Institutes of Health). Images were further processed in Adobe Photoshop CS3. Figure plates and schematic representations were created with Adobe Illustrator CS3.

3. Results

3.1. Overview of developmental characteristics in C. teleta

A detailed staging system of *C. teleta* has been published previously (Seaver et al., 2005) and will only be briefly summarized here. The early spiral cleavages represent stage 1, followed by late cleavage and gastrulation that are designated stage 2 and 3, respectively. At stage 4, about 2 days after fertilization, larvae start to show the first morphologically distinct features (Fig. 1A, E). The following developmental stages last about 1 day each: 3 days of development is stage 5 (Fig. 1B, F), 4 days of development is stage 6 (Fig. 1C, G), and 5 days of development is stage 7 (Fig. 1D, H). At stage 9, about 7–8 days after fertilization, larval development is complete and metamorphosis can be induced. In larvae with labeled nuclei (Fig. 1A–D), the prototroch (pt), telotroch (tt) and stomodeum (st) appear as regions of lower nuclear density. The prototroch and telotroch are ciliary bands that run around the circumference of the larvae just posterior of the head and anterior of the pygidium, respectively, and these prominent features are useful landmarks. Another landmark is the stomodeum, which also possesses cilia. The cilia are heavily labeled with anti-acetylated α-tubulin (Fig. 1E–H) and therefore all landmarks are clearly visible. Stage 4 larvae show lateral segment anlagen (Fig. 1A, open arrow) that will form the trunk segments and become visible in stage 5 larvae (Fig. 1B–D, brackets). Segmentation starts in the ventral lateral region (Seaver et al., 2005), leaving an

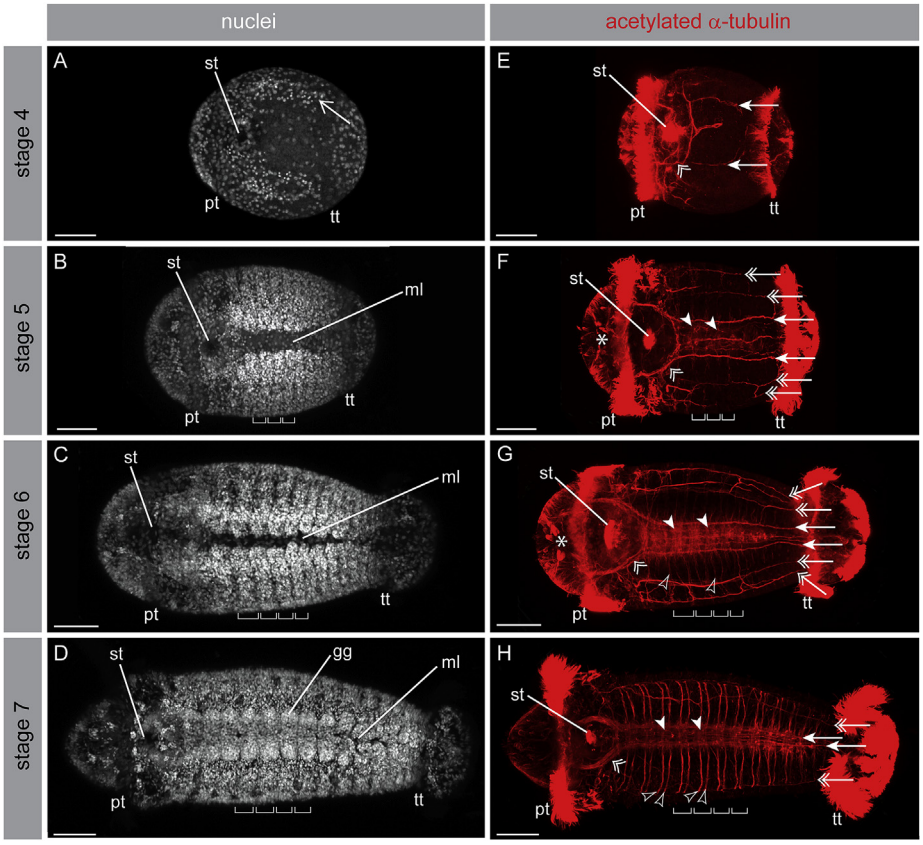

Fig. 1. Characteristics of *C. teleta* larvae. Hoechst staining labels nuclei in white (nuclei; A-D) and anti-acetylated α-tubulin staining labels axon projections and cilia in red (a-tub^{+} NS; E-H). The images in each row are from the same individual, and all images are ventral views. Four different larval stages are shown: stage 4 (A, E), stage 5 (B, F), stage 6 (C, G), and stage 7 (D, H). All images are z-stack projections, with anterior to the left. The open arrow in A shows the location of the segment anlagen. The brackets in B, C, D, F, G and H represent the width of individual segments. The double open arrowheads in E–H point to the circumoral nerves. The main connectives of the ventral nerve cord are indicated by the arrows in E-H, while double open arrows point towards the lateral longitudinal nerves. In F–H, filled arrowheads indicate two sets of commissures in the ventral nerve cord. Unfilled arrowheads highlight selected individual segmental nerves in F–H. The asterisks in F and G mark the position of the anti-acetylated α-tubulin positive neurons in the head. Abbreviations: gg: ganglia, ml: ventral midline, pt: prototroch, st: stomodeum, tt: telotroch. Scale bars: 50 μm.

unsegmented ventral midline (ml). Over time the segments expand dorsally and ventrally, and the unsegmented ventral midline successively gets more restricted (compare Fig. 1B, C and D). After complete closure of the ventral midline in the anterior trunk at stage 7, ganglia become visible (Fig. 1D, gg). A detailed description of the development and architecture of the nervous system in *C. teleta* has been published (Meyer et al., 2015). The first distinct anlagen of the central nervous system, the circumoral nerves (Fig. 1E–H, double open arrowheads) and main longitudinal connectives (Fig. 1E–H, arrows) appear at stage 4. Further maturation of the ventral nerve cord includes the addition of commissures at stage 5 (Fig. 1F–H, filled arrowheads) and segmental nerves at stage 6 (Fig. 1G and H, unfilled arrowheads). The latter are characteristic components of the peripheral nervous system, as are the lateral longitudinal nerves that run along the trunk, two on each side (Fig. 1F–H, double open arrows). Anterior to the brain is a bilateral cluster of anti-acetylated α-tubulin positive neurons, comprising three neurons on each side (Fig. 1F and G, asterisks).

The eyes in *C. teleta* are rather simple, and are comprised of only three different cell types: a pigment, sensory, and supporting cell (Rhode, 1993). The antibody 22C10 specifically labels sensory cells associated with the eyes in *C. teleta* (magenta in Fig. 2A', A'', B′, B'', C′, C''). Previous studies have demonstrated that the sensory neuron of the eye is distinctively labeled by 22C10 in annelids, such as in *C. teleta* (Yamaguchi and Seaver, 2013) and *Platynereis massiliensis* (Helm et al., 2014). The head region of older *Capitella* larvae (starting at late stage 5) has two bilateral 22C10 positive domains on each side of the head, an anterior sensory cell (magenta in Fig. 2A', A'', B′, B'', C′, C'', unfilled arrowheads) and a posterior sensory cell (magenta in Fig. 2A', A'', B′, B'', C′, C'', filled arrowheads). The anterior sensory cell (Fig. 2A, B, C, unfilled arrowheads) is situated medially within the brain (Fig. 2C, dotted yellow line), while the posterior sensory cell (Fig. 2A, B, C, filled arrowheads) is located towards the lateral-posterior edge of the brain. Double labeling experiments with *Ct-r-opsin1* (yellow in Fig. 2A', A‴, B′, B‴) and the 22C10 antibody (magenta in Fig. 2A', A'', B′, B''), clearly show co-localization (Fig. 2A', B′), indicating the specificity of anti-22C10 to label photo-sensory cells in *C. teleta*. Fine neural processes from both the anterior and posterior sensory cell extend medially and appear to meet each other to form a single projection, which ends in an agglomeration straddling the midline of the brain (Fig. 2C-C'''; Fig. 9E, arrows). Comparison with anti-serotonin labeling (green in Fig. 2C', C‴) reveals that the 22C10-positive projections are within the main cerebral commissure of the brain. This is in contrast to the situation found in the annelid *P. dumerilii*, where there is a direct axonal contact between the eyespots and the prototroch (Jékely et al., 2008). The posterior sensory cell is in contact with the pigment cell of the larval eye (Yamaguchi and Seaver, 2013) (Fig. 9A, double open arrowheads), and the pigment cell is situated close to the prototroch at the lateral-posterior portion of the brain. The anterior 22C10-labeled cell is thought to be the progenitor of the juvenile eye as the posterior cell is lost at metamorphosis (Yamaguchi and Seaver, 2013).

3.2. *Ct-pax6 is expressed in distinct subdomains of the nervous system and the eye*

A previous paper identified one *pax6* orthologue in the *C. teleta* genome (Seaver et al., 2012), which encodes two highly conserved DNA-binding domains, a bipartite paired domain and a paired-type homeodomain, and a C-terminal proline-serine-threonine (PST)-rich transactivation domain. A recent study of genome wide searches for homeodomain-containing genes in annelids reported a second *pax6*-like gene in the genome of *C. teleta* (Zwarycz et al., 2015), which is in line with other recent findings in several non-mammalian vertebrate species (Ravi et al., 2013). However, this putative second *pax6* gene, *pax6.2*, encodes only a Pax6-like homeodomain, but not a paired domain characteristic of genes belonging to the *pax6* family. Multiple attempts to amplify this second *pax6* gene from various cDNA templates representing

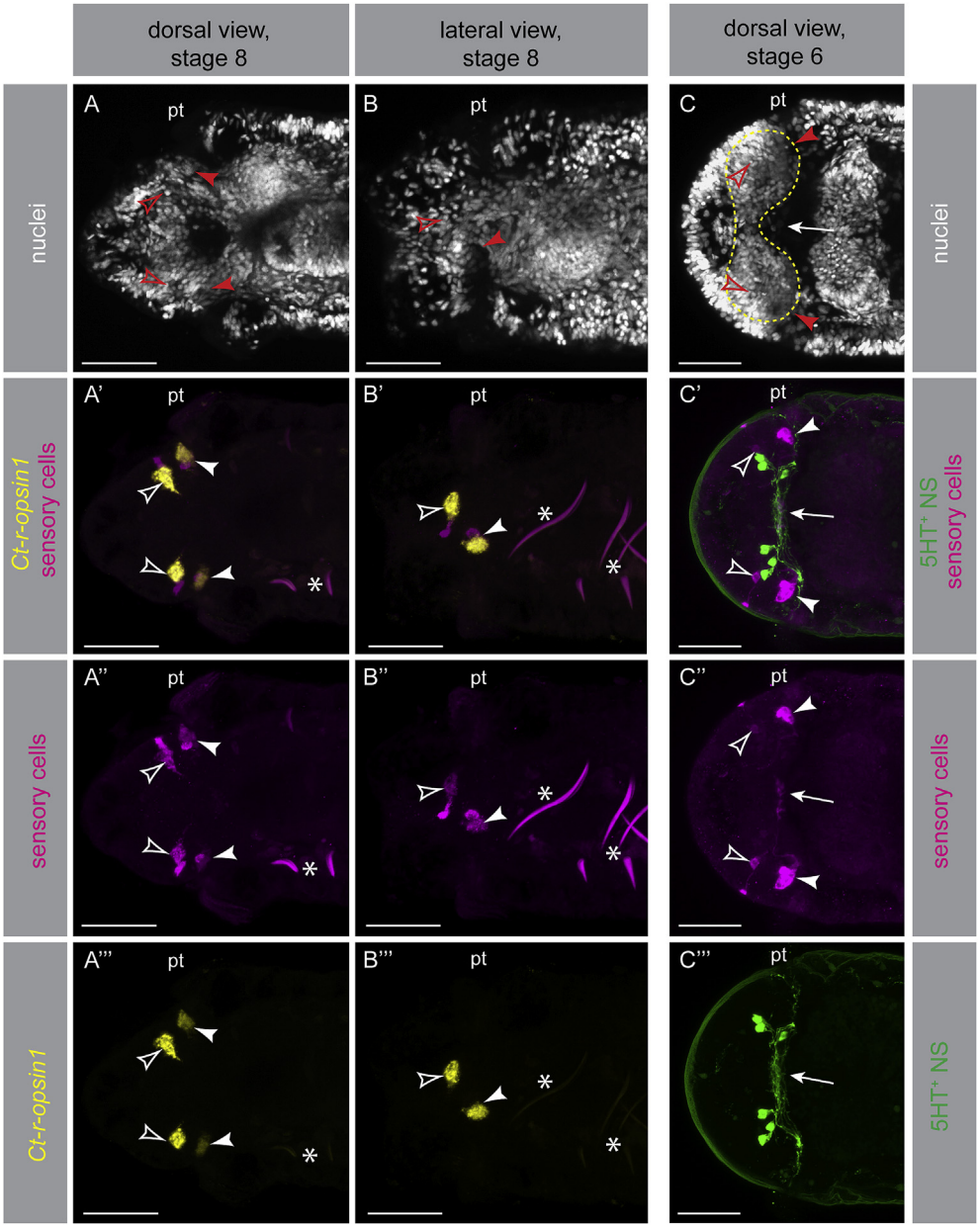

Fig. 2. Characteristics of the eyes in *C. teleta* larvae. Hoechst staining labels nuclei in white (nuclei; A, B, C), *Ct-r-opsin1* whole mount *in situ* expression in yellow (*Ct-r-opsin1*; A′, A‴, B′, B‴), 22C10 antibody labeling of the sensory cell of the eye in magenta (sensory cells; A′, A′′, B′, B′′, C′, C′′), and serotonin antibody labeling of neural projections in green (5HT^{+} NS; C′, C‴). A′, B′ and C′ are merged channels of A′′ plus A‴, B′′ plus B‴, and C′′ plus C‴, respectively. The images shown are z-stack projections of the head-region, with anterior to the left. Images from each column are from the same individual. There are two photo-sensory cells, an anterior sensory cell (unfilled arrowheads) and a posterior sensory cell (filled arrowheads). The arrow marks the region where the neural projections of the sensory cells meet (C–C‴). Segmentally iterated chaetae of the trunk are autofluorescent and therefore visible in some of the 22C10 images (asterisks). Abbreviation: pt: prototroch. Scale bars: 30 μm.

different stages of development were unsuccessful, and therefore this putative second *pax6* gene does not appear to be transcribed. From this observation, together with the fact that the predicted protein lacks a paired domain, we deduce that *C. teleta* has a single functional *pax6* orthologue, which we denote as *Ct-pax6*.

The wildtype expression pattern of *Ct-pax6* in *C. teleta* was investigated using *in situ* hybridization (Figs. 3 and 4). *Ct-pax6* transcript is not detectable during early cleavage and gastrulation stages (data not shown). The earliest detectable *Ct-pax6* expression is at larval stage 3, where the transcript is found in two small bilateral domains in the anterior ectoderm (data not shown). In early larval stage 4, the main expression domain of *Ct-pax6* is in the developing brain lobes (Fig. 3A, asterisk). In addition, there are a few scattered *Ct-pax6*-positive cells in the anlagen of the ventral nerve cord (Fig. 3A, filled arrowheads). This onset of *Ct-pax6* expression correlates with the appearance of differentiated neurons in the brain and the main nerves of the central nervous system, including a nerve connecting the two brain lobes, the circumoral nerves and the main longitudinal connectives (see Fig. 1E and (Meyer et al., 2015)). By larval stage 5, *Ct-pax6* expression in the brain lobes has broadened medially and posteriorly (Fig. 3B, asterisk). The ventral nerve cord now exhibits segmentally iterated stripes of expression (Fig. 3B, black arrows). Brain expression in stage 6 larvae starts to segregate into a lateral (Fig. 3C, asterisk) and a medial (Fig. 3C, double open arrowhead) subdomain. Even more cells of the ventral nerve cord express *Ct-pax6*, and expression spans the length of the trunk. Nevertheless, segmental stripes are clearly visible in the anterior four to five segments (Fig. 3C', black arrows), while the expression in the posterior is denser. This pattern likely reflects the anterior to posterior temporal progression of ganglia formation in the ventral nerve cord. There is a clear distinction of the *Ct-pax6* brain expression into subdomains at larval stage 7, a lateral (Fig. 3D, asterisk), a medial (Fig. 3D, double open arrowhead) and a ventral expression domain (Fig. 3D, double open arrow). Expression in discrete subsets of cells in the ventral nerve cord has become more pronounced, displaying a segmentally iterated pattern of short lateral, diagonal stripes (Fig. 3D', black arrows) and medial spots (Fig. 3D', white arrows) in the anterior segments. Apart from the predominate expression of *Ct-pax6* in elements of the central nervous system, a few isolated cells in the posterior 2/3 of the trunk ectoderm (Fig. 3D', unfilled arrowheads)

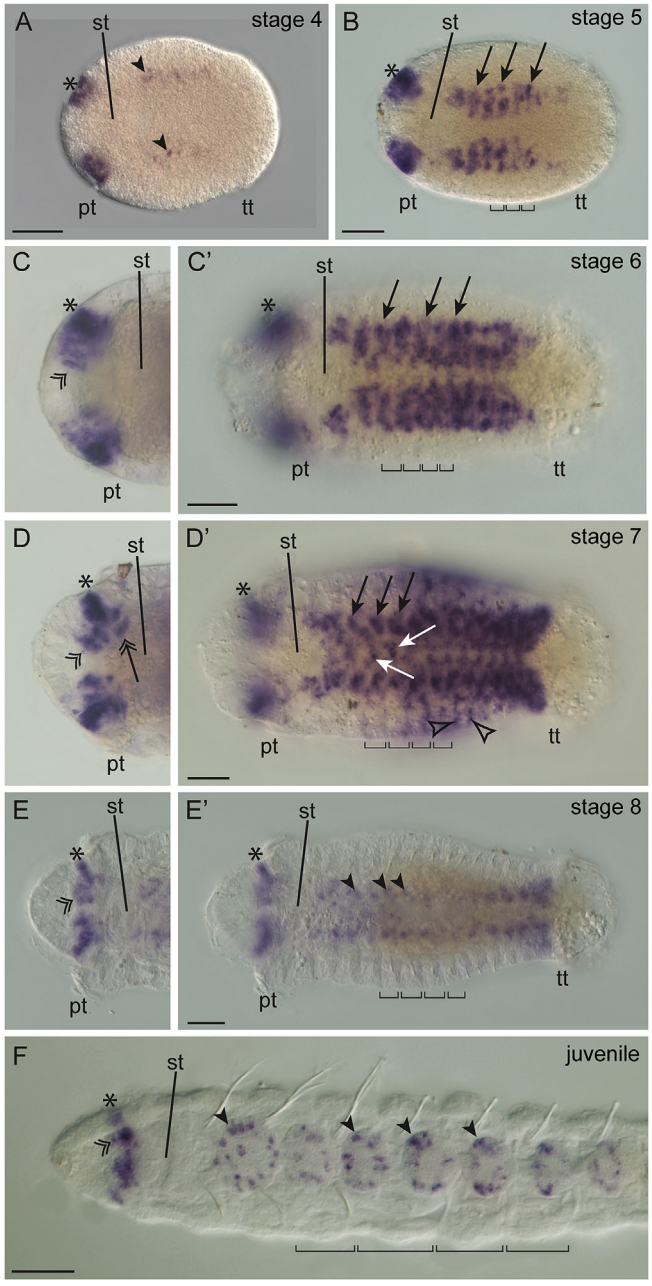

Fig. 3. Expression of *Ct-pax6* in the nervous system. Colorimetric whole mount *in situ* for *Ct-pax6* (dark purple). Six different stages are shown: larval stage 4 (A), larval stage 5 (B), larval stage 6 (C, C′), larval stage 7 (D, D′), larval stage 8 (E, E′), and 12 day juvenile (F). All images are composites of multiple focal planes (Helicon Focus software), with anterior to the left. The brackets in B, C′, D′, E′ and F represent the width of individual segments. Note that there is a slight discordance in juvenile stages between the external segmentation (marked by the aforementioned brackets) and the internal segmentation of the nervous system (ganglia). The lateral region of the brain is indicated by asterisks (A–F), while the medial portion is designated by double open arrowheads (C–F) and the posterior region is highlighted with the double open arrow (D). *Ct-pax6* is expressed in the ventral nerve cord. At early and late stages, expression is restricted to a few cells (A, E′, F, filled arrowheads). Segmentally-repeated lateral diagonal stripes (B, C′, D′, black arrows) and medial spots (D′, white arrows) are distinguishable during the peak phase of *Ct-pax6* expression in the ventral nerve cord. *Ct-pax6* expression is visible outside the central nervous system in stage 7 larvae (D′, unfilled arrowheads) Abbreviations: pt: prototroch, st: stomodeum, tt: telotroch. Scale bars: 50 μm.

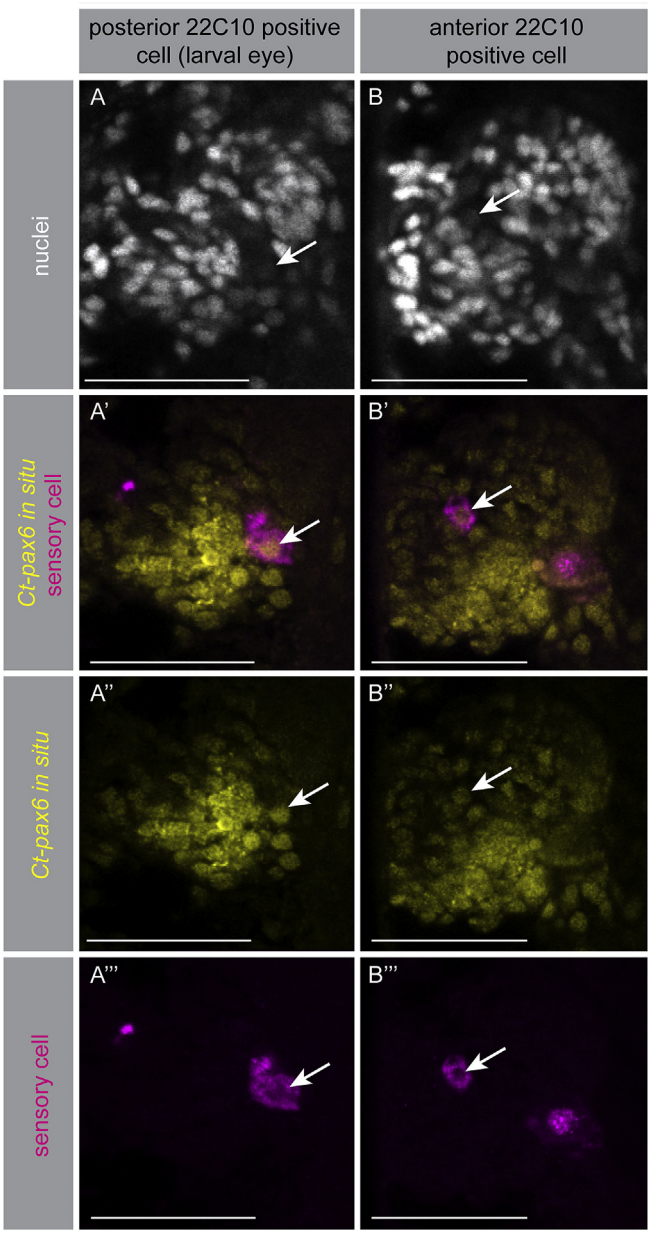

Fig. 4. Ct-*pax6* expression in the eye of *C. teleta* larvae. Hoechst staining to label nuclei in white (nuclei; A, B), *Ct-pax6* whole mount *in situ* expression in yellow (*Ct-pax6*; A′, A′′, B′, B′′) and 22C10 antibody labeling of the sensory cell of the eye in magenta (sensory cells; A′, A′′′, B′, B′′′). A′ and B′ are merged channels of A′′ plus A′′′ and B′′ plus B′′′, respectively. The images shown are high magnification views of the brain-region of stage 6 larvae, with anterior to the left. Each image represents a single confocal slice only. Images from each column are from the same individual. A sub-region of both sensory cells expresses *Ct-pax6* (highlighted by arrows). Scale bars: 30 μm.

also express the transcript. Although elements of the peripheral nervous system have not been mapped carefully in *C. teleta*, the position of these *pax6*-positive cells might indicate that they are a part of the peripheral nervous system. A number of neurogenic genes, such as *prospero*, *soxB1*, and *soxB* have been shown to have similar expression patterns (Sur et al., 2017), supporting the idea that the peripheral nervous system develops in this trunk region. After the prominent expression of *Ct-pax6* at stage 6 and 7, transcription is down regulated at larval stage 8 (Fig. 3E, E′). This holds true for the bipartite brain expression (Fig. 3E, asterisk and double

open arrowhead) as well as the ventral nerve cord, where expression is most pronounced in the lateral portion of the ganglia (Fig. 3E', filled arrowheads), with a few scattered cells in more medial positions. At larval stage 9, *Ct-pax6* expression is reduced further, with very small lateral and medial subdomains in the brain, and almost no expression in the ventral nerve cord (data not shown). Juvenile worms show a similar pattern of anterior *Ct-pax6* expression as in the larvae, a lateral (Fig. 3F, asterisk) and a medial (Fig. 3F, double open arrowhead) subdomain. Isolated, segmentally repeated cells within the ganglia of the ventral nerve cord are *Ct-pax6*-positive in juveniles (Fig. 3F, filled arrowheads).

To examine if *Ct-pax6* was expressed in the larval photo-sensory cells, we combined *Ct-pax6 in situ* hybridization (yellow in Fig. 4A', A'', B′, B'') and 22C10 antibody labeling (magenta in Fig. 4A', A‴, B′, B‴), which specifically labels sensory cells associated with the eyes in *C. teleta* (see above). In larvae older than stage 5, there are two sensory cells on each side of the head, an anterior and a posterior sensory cell, and both have their cell bodies within the brain lobes (Fig. 4A and B, arrows, weakly stained). Many brain cells are *Ct-pax6*-positive (yellow in Fig. 4A', A'', B′, B''), and *Ct-pax6* is also expressed within each of the sensory cells (magenta in Fig. 4A', A‴, B′, B‴, arrows), indicating expression in the larval photoreceptors.

To summarize, *Ct-pax6* is expressed in distinct subdomains in the developing brain and ventral nerve cord of *C. teleta* larvae and juveniles. Additionally, both pairs of photo-sensory cells present in the larval head express *Ct-pax6*.

3.3. Experimental strategy and morpholino validation

To investigate function of *Ct-pax6* during development, a morpholino knockdown approach was taken. The pre-spliced *Ct-pax6* mRNA consists of ten exons and nine introns (Fig. 5A). This number of exons found in the *Ct-pax6* gene is similar to what has been reported in various other species (Chisholm and Horvitz, 1995; Glardon et al., 1997; van Heyningen and Williamson, 2002). The paired box spans two exons, namely exon 3 and exon 4 (magenta in Fig. 5), while the homeobox spans three exons, namely exon 5, exon 6, and exon 7 (green in Fig. 5).

For the morpholino (MO) knockdown experiments, a translation-blocking MO and two different splice-blocking morpholinos were designed to target the two different DNA-binding motifs of *Ct-pax6*, the paired domain and paired-type homeodomain. One morpholino, "MO-1", binds to the second exon-intron-boundary (blue in Fig. 5A, top schematic). Sufficient splice-blocking activity of MO-1 results in the inclusion of the second intron (Fig. 5B, right schematic), which would introduce 48 missense amino acids before reaching a premature stop codon in the modified post-spliced mRNA (Fig. 5B, blue asterisk in right schematic). This means that if a protein is synthesized, it would contain neither a paired domain nor a homeodomain. In contrast, the second morpholino, "MO-2", binds to the fourth exon-intron-boundary (orange in Fig. 5A, top schematic). Sufficient splice-blocking activity of MO-2 results in the inclusion of the fourth intron (Fig. 5C, right schematic), which would introduce 17 missense amino acids before reaching a premature stop codon in the modified post-spliced mRNA (Fig. 5C, orange asterisk in right schematic). In this case, the paired domain would be retained in the modified, truncated protein, but the DNA-binding homeodomain would be missing. Additionally, a translation-blocking morpholino, "MO-trans", was designed to block translation at the start codon, and therefore would result in the absence of Pax6 protein.

To check for potential off-target binding sites to mRNA sequences by all employed morpholinos, a Blast search against the publicly available *Capitella teleta* genome was performed. It is generally assumed that a five base pair mismatch spread throughout a 25-mer morpholino (typical length) results in a loss of knockdown activity (Eisen and Smith, 2008). Every sequence with a significant alignment was investigated in detail since the activity of morpholinos are highly specific to either block translation (when targeted to the 5' UTR or first 25 base pairs of coding sequence) or splicing (when targeted in introns near intron-exon boundaries). Morpholino homology to an off-target mRNA outside of these limited regions is unlikely to affect the expression of the off-target mRNA (Gene Tools). Taking all these considerations into account, we found that neither of the two control morpholinos is likely to bind and initiate a gene knockdown of any mRNA in *C. teleta*. Morpholinos specific to *Ct-pax6* show a 100% sequence homology with scaffold 29 only, which is the scaffold in which *pax6* is located. No other off-target mRNA binding sites that would affect gene expression could be found, including the potential second *Ct-pax6* gene, *pax6.2*, which is located on scaffold 38209.

RT-qPCR was used to validate the efficiency of both splice-blocking morpholinos. For each morpholino, two sets of specific primers were designed. One primer set was used to evaluate the level of spliced *Ct-pax6* transcript: F1&R1 for MO-1 and F3&R3 for MO-2 (Fig. 5A, middle schematic). A second primer set was used to examine the level of unspliced *Ct-pax6* transcript: F2&R2 for MO-1 and F4&R4 for MO-2 (Fig. 5A, middle schematic). Fold changes of relative *Ct-pax6* transcript levels were calculated (using *Ct-HPRT* as reference gene) and are displayed on a logarithmic scale in Fig. 5B and C. Three experimental treatment groups were compared: larvae resulting from *Ct-pax6* MO injections (blue bars in Fig. 5B and C), larvae resulting from control MO injections (red bars in Fig. 5B and C), and larvae resulting from uninjected embryos (light green bars in Fig. 5B and C). There are no statistically significant differences in *Ct-pax6* transcript levels between the control MO injected larvae and the uninjected larvae for all four primer pairs: F1&R1 with $p = 0.26099$, F2&R2 with $p = 0.19828$, F3&R3 with $p = 0.29864$, and F4&R4 with $p = 0.58846$ (two-tailed Student's *t*-test). This shows that neither the injection process, nor the use of a generic standard control morpholino perturb the wildtype expression levels of *Ct-pax6* transcript in *C. teleta* larvae. There is a statistically significant down-regulation of correctly spliced *Ct-pax6* transcript in MO-1 injected larvae ($p = 0.00462$, one-tailed Student's *t*-test) (Fig. 5B, left side of bar graph, F1&R1). Furthermore, the unspliced *Ct-pax6* transcript is significantly up-regulated in MO-1 injected larvae ($p = 0.00947$, one-tailed Student's *t*-test) (Fig. 5B, right side of bar graph, F2&R2). Larvae resulting from injections of MO-2 show a higher variability in *Ct-pax6* transcript levels than larvae injected with MO-1. Although there is no statistically significant difference ($p = 0.07667$, one-tailed Student's *t*-test), a nearly 2-fold down-regulation of the correctly spliced *Ct-pax6* transcript in MO-2 injected larvae is seen when compared to larvae resulting from control MO injections (Fig. 5C, left side of bar graph, F3&R3). In contrast, a statistically significant up-regulation of the unspliced *Ct-pax6* transcript is detected in larvae resulting from MO-2 injections ($p = 0.01317$, one-tailed Student's *t*-test) (Fig. 5C, right side of bar graph, F4&R4). Transcript could not be detected in any of the -RT-control samples (5 primer pairs tested: 4 experimental and the reference gene), demonstrating that there is no contamination with residual genomic DNA in any of the experimental samples. This control validates that the statistically significant up-regulation of both unspliced transcripts following MO injection is a real signal. The efficiency of the translation-blocking MO could not be tested using RT-qPCR as the *Ct-pax6* mRNA will not be altered by this morpholino.

Phenotypic analysis of larvae resulting from injections with different morpholinos resulted in different phenotypes that could be classified into five distinct categories (Fig. 6), with increasing severity levels ranging from one to five. Category I larvae exhibit normal general morphology, but show a nervous system phenotype. Category II larvae are elongated but have malformations in their general morphology (such as a bent body axis, or disrupted segmentation) and also show a nervous system phenotype. In the case of category III larvae, injected embryos developed into larvae with many normal morphological features, but they failed to develop segment boundaries or fully elongate their trunk, and the ganglia of the ventral nerve cord did not condense. In addition, most category III larvae also show malformations in their central and peripheral nervous system architecture. Injected animals that completed gastrulation and had a round morphology with cilia and sometimes differentiated

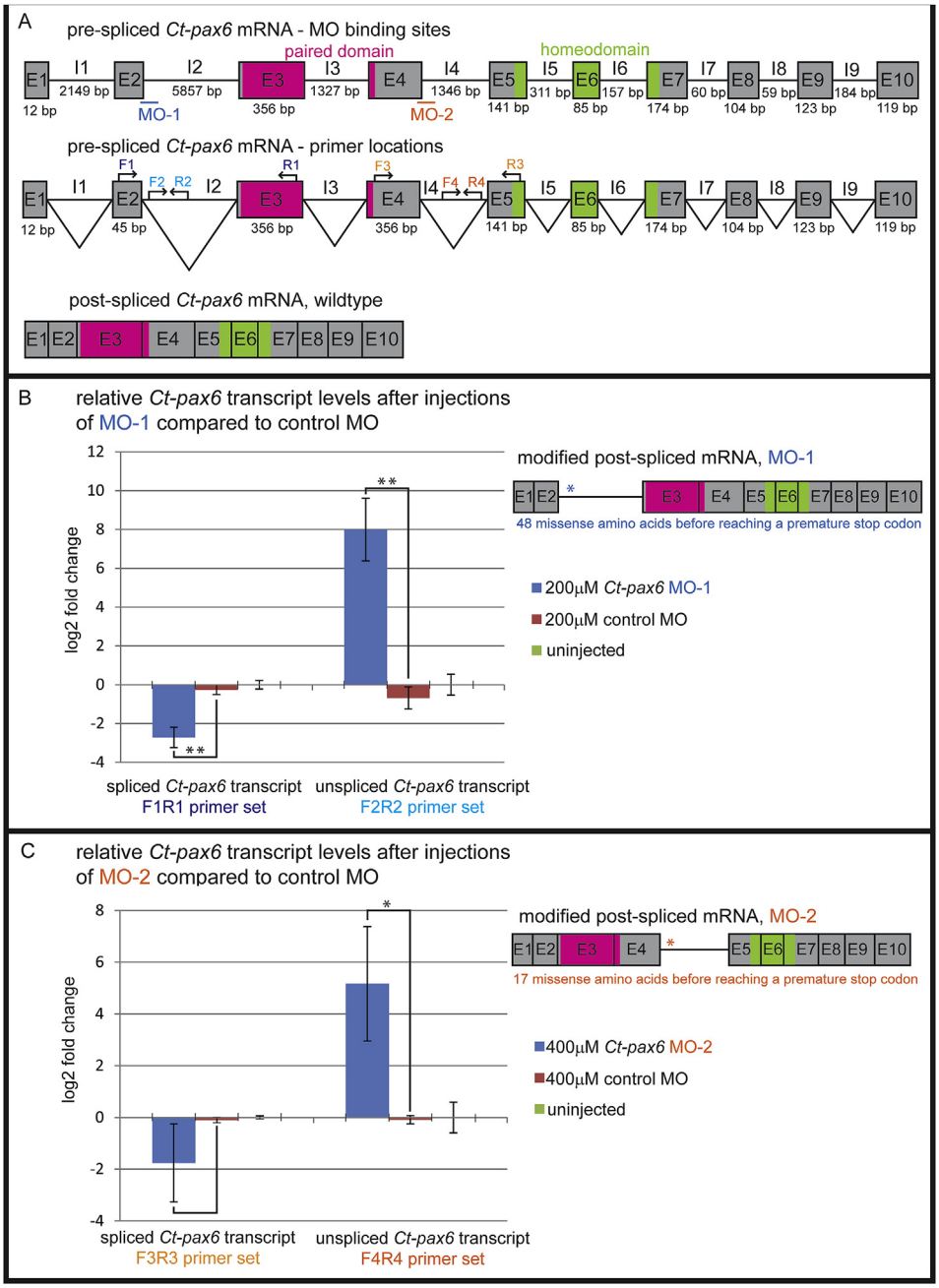

Fig. 5. Experimental strategy and validation of the morpholino experiments. Schematic and graphic display of the splice-blocking morpholino (MO) strategy employed (A) and validation (B, C). Exons are represented by boxes that include the corresponding exon-number (E1 to E10). Introns are represented by lines with the corresponding intron-number above (I1 to I9). The size in base pairs (bp) of each exon and intron is shown underneath the box or line, respectively. The positions of the DNA-binding domains are marked, with the paired box in magenta and the homeobox in green. Elements associated with MO-1 are blue, while MO-2 associated elements are orange. (A) Morpholino strategy. The top schematic shows the organization of pre-spliced *Ct-pax6* mRNA with the location of the target sites of both splice-blocking morpholinos. MO-1 is at the second exon-intron-boundary and MO-2 is at the fourth exon-intron-boundary. The positions of the primer sets (F1&R1, F2&R2, F3&R3, and F4&R4) used to analyze the efficiency of splice blocking by the two MOs are indicated in the middle schematic. The bottom schematic depicts the wildtype post-spliced *Ct-pax6* mRNA. (B) Relative *Ct-pax6* transcript levels after injections of MO-1 (blue) compared to control MO (red). The bar graph shows the down-regulation of correctly spliced *Ct-pax6* transcript (left side) as well as the up-regulation of the unspliced *Ct-pax6* transcript (right side). The error bars on each column represent standard deviation. Note that a logarithmic scale is shown. Statistical significance where $p = \leq 0.01$ is denoted by **, *p* values were calculated using a one-tailed Student's *t*-test. The schematic on the right displays the modified post-spliced *Ct-pax6* mRNA after MO-1 injections, which results in the inclusion of the second intron. The asterisk marks the positions of premature stop codons included through modified splicing due to MO activity. (C) Relative *Ct-pax6* transcript levels after injections of MO-2 (blue) compared to control MO (red). The bar graph (logarithmic scale) shows the down-regulation of correctly spliced *pax6* transcript (left side) as well as the up-regulation of the unspliced *pax6* transcript (right side). The up-regulation is statistically significant: * $\leq$ 0.5; *p* value calculated using a one-tailed Student's *t*-test. The schematic on the right displays the modified post-spliced *pax6* mRNA after MO-2 injections, which results in the inclusion of the fourth intron. The asterisk marks the positions of premature stop codons included through modified splicing due to MO activity.

neurons, were designated category IV. Injected animals that did not complete early cleavages or gastrulate, and resulted in arrested development were defined as category V.

Because this is the first time MOs have been used to disrupt gene expression in *C. teleta*, we determined a suitable concentration for sufficient MO activity, including the standard control MO. To assess general toxicity of morpholinos on the development of *C. teleta* larvae, four increasing concentrations of the control MO were tested (Suppl. Fig. 2). The majority of 100 µM, 200 µM, 300 µM, and 400 µM control MO injected embryos developed normally, resulting in wildtype phenotypic larvae (Suppl. Fig. 2, light blue portion of the bars). It can therefore be concluded that injection of a morpholino into uncleaved *Capitella* embryos is not toxic at these concentrations, since the general development of the embryos/larvae is not negatively affected. Judgment on the appropriate concentration of MO-1 was based on a morphological analysis. Four concentrations of MO-1 were tested to find a balance between phenotypes too severe to be informative (MO concentration too high) and insufficient MO activity (MO concentration too low): 100 µM, 200 µM, 300 µM, and 400 µM (Suppl. Fig. 3). Injections of 100 µM MO-1 resulted in a majority of larvae with a wildtype phenotype (blue portion of the first bar in Suppl. Fig. 3B). In contrast, microinjection of 300 µM and 400 µM of MO-1 resulted in severe phenotypes, since the majority of larvae showed either a category IV or V phenotype (orange and magenta portion of the third and fourth bar in Suppl. Fig. 3B). 200 µM MO-1 was chosen as the appropriate MO-1 concentration for more detailed analyses due to a reasonable balance of resulting phenotypes (Fig. 6B, first bar; Suppl. Fig. 3B, second bar): a high proportion of larvae exhibited a category III phenotype (56%, $n = 104/186$), a low proportion of category

A

	200 µM *Ct-pax6* MO-1		200 µM *Ct-pax6* MO-trans		200 µM control MO		200 µM mismatch MO		400 µM *Ct-pax6* MO-2		400 µM control MO	
	n	%	n	%	n	%	n	%	n	%	n	%
total	186		126		252		96		227		160	
wildtype	28	15	10	8	198	79	46	50	35	15	145	90
category I	0	0	4	3	4	2	19	20	66	29	1	1
category II	11	6	4	3	18	7	11	11	91	40	5	3
category III	107	58	50	40	5	2	6	6	2	1	3	2
category IV	34	18	18	14	25	10	12	12	29	13	6	4
category V	6	3	40	32	2	1	2	2	3	1	0	0

B

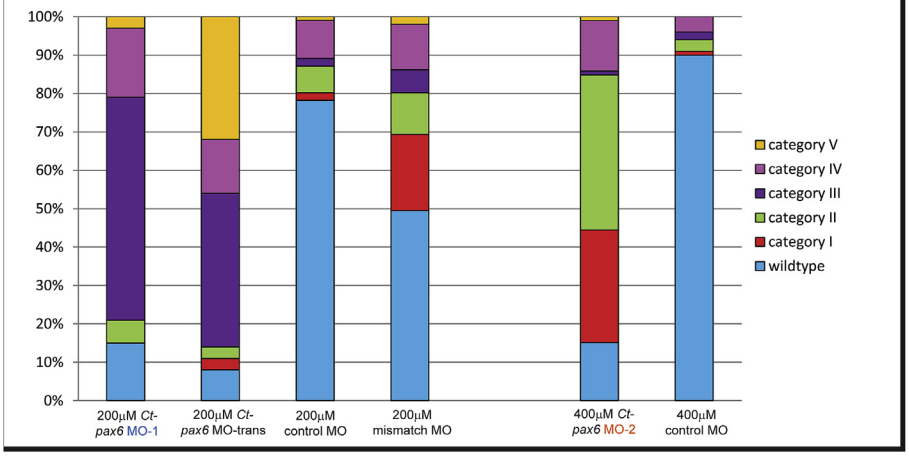

Fig. 6. Summary of phenotypic characteristics after MO injections. Phenotypic analysis of larvae resulting from injections with 200 µM MO-1, 200 µM MO-trans, 200 µM mismatch MO or 400 µM MO-2 morpholino resulted in a variety of different phenotypes which could be classified into five distinct categories. Panel A shows data in table format including *n* numbers, and panel B shows graphic representation of the same data. Category I larvae exhibit normal general morphology, but show a nervous system phenotype (red portion of bars). Category II larvae are elongated but have malformations in their general morphology and also show a nervous system phenotype (green portion of bars). Category III larvae exhibit malformations in their central and peripheral nervous system architecture (purple portion of bars). Injected animals that completed gastrulation, and then formed a ball of gastrulated cells with cilia, were designated category IV (magenta portion of bars). Injected animals that did not complete early cleavages but resulted in an arrested development, were defined as category V (orange portion of bars). Larvae resulting from injections of either 200 µM MO-1 as well as 200 µM MO-trans show a very similar distribution of phenotypic categories, with the predominate being category III (first and second bars). The control morpholinos, the mismatch MO and different concentrations of the standard control MO, result in mainly wildtype phenotypic larvae (blue portion of third, fourth and sixth bar). Larvae resulting from injections with 400 µM MO-2 exhibit category I and II as the predominate phenotypic categories (fifth bar).

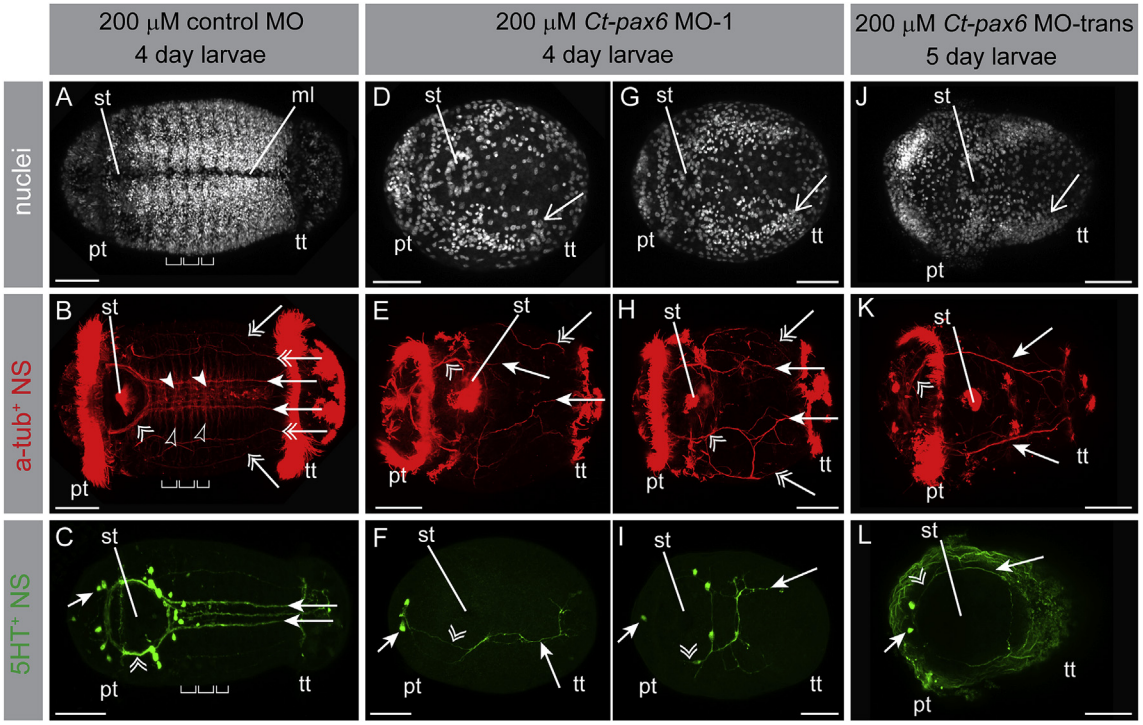

Fig. 7. Phenotype of *C. teleta* larvae after MO-1 and MO-trans injections. Hoechst staining labels nuclei in white (nuclei; A, D, G, J), anti-acetylated α-tubulin labeling in red (a-tub^{+} NS; B, E, H, K) and anti-serotonin labeling in green (5HT^{+} NS; C, F, I, L). The images in A-C, D-F, G-I and J-L are from the same individual. The developmental time for 200 µM control and 200 µM MO-1 larvae shown is four days, that for 200 µM MO-trans is five days. All images are z-stack projections, with anterior to the left. The open arrows in D, G, and J show the location of the segment anlagen. The brackets in A-C and I represent the width of individual segments. The double open arrowheads in B, E, H and K point towards the circumoral nerves. The main connectives of the ventral nerve cord are indicated by the long arrows in B, E, H, and K, while lateral longitudinal nerves are highlighted by double open arrows. The commissures (filled arrowheads) and selected individual segmental nerves (unfilled arrowheads) of the ventral nerve cord are highlighted in B. The short arrows in C, F, I and L mark the position of serotonin positive neurons in the brain. Abbreviations: ml: ventral midline, pt: prototroch, st: stomodeum, tt: telotroch. Scale bars: 50 µm.

V animals (3%, $n = 6/186$), and moderate proportion of either category IV animals (18%, $n = 34/186$) or wildtype larvae (15%, $n = 28/186$). The majority of the larvae resulting from injection of 200 μM control MO (74%, $n = 198/252$) developed into wildtype larvae (Fig. 6B, blue portion of the third bar).

To verify the phenotypic specificity of MO-1, we injected the corresponding mismatch MO. Here, a loss of knockdown activity is achieved by spreading five mismatched bases throughout the length of the morpholino. In the following two morpholino sequences, mismatched bases in the mismatch MO are underlined and highlighted in bold: 5′ AAcGcAAGAcGAGAcCCTAgCTCTC 3' (mismatch MO for MO-1) and 5′ AAGGGAAGAGGAGAGCCTACCTCTC 3' (MO-1). The majority of larvae resulting from injections of 200 μM mismatch MO (70%, $n = 65/96$) are either wildtype or phenotypically wildtype with slight alterations in the nervous system (Fig. 6B, blue and red portions of the forth bar; Suppl. Fig. 4). In contrast to MO-1, only a small proportion of the mismatch MO (6%, $n = 6/96$) developed into the MO-1 characteristic category III larvae (Fig. 6B, purple portion of the forth bar). This highly suggests that the phenotypic development of larvae injected with 200 μM MO-1 is due to the absence of normal Pax6 protein.

To add further evidence, we analyzed larvae resulting from injections of a 200 μM Ct-pax6 translation-blocking MO. Injections with the translation-blocking MO would not contain either the paired domain or homeodomain, and the DNA binding properties of this altered Ct-Pax6 protein are expected to be eliminated. This would be similar to the situation for injection of MO-1. Indeed, injections of 200 μM MO-trans result in a substantial proportion (40%, n = 50/126) of larvae with a category III phenotype (Fig. 6B, purple portion of the second bar; Fig. 7J, K, L).

The appropriate concentration of MO-2 was determined by analysing levels of correctly spliced *Ct-pax6* transcript via RT-qPCR using the primer set F3&R3 (Fig. 5A, middle schematic). Although injections of 200 μM MO-2 did not result in reduction of the correctly spliced *Ct-pax6* transcript (log2 fold change −0.02389), a moderate down-regulation of the correctly spliced *Ct-pax6* transcript was achieved with a concentration of 300 μM MO-2 (log2 fold change −1.36907). Injections of 400 μM MO-2 was found to be suitable for the remaining experiments with an average log2 fold change of −1.76044. 400 μM MO-2 injections into uncleaved eggs results in two prominent phenotypes: categories I (29%, $n = 66/227$) and II (40%, $n = 91/227$) (red and green portions of the fifth bar in Fig. 6B).

3.4. Nervous system phenotype after Ct-pax6 knockdown

Analysis of larvae resulting from injections with 200 μM MO-1 (Fig. 6A; 56%, $n = 104/186$) and 200 μM MO-trans (Fig. 6A; 40%, $n = 50/126$) show category III to be the predominate phenotype. This phenotype is only seen in larvae resulting from injections with 200 μM MO-1 (Fig. 7D – I) or 200 μM MO-trans (Fig. 7J – L), but not in larvae resulting from injections with 200 μM control MO (Fig. 7A – C). Category III larvae possess a number of morphological features typical of a stage 4 larva (Fig. 1A, E): a prototroch, telotroch, and stomodeum as well as segment anlagen in the ventral lateral region (Fig. 7D, G, J open arrows). However, these larvae have not undergone elongation of the anterior-posterior body axis and lack all signs of segmentation in the trunk region. Antibodies against acetylated *α*-tubulin (Fig. 7B, E, H, K), serotonin (Fig. 7C, F, I, L) and FMRFamide (data not shown) were used to assess the development of the nervous system in larvae resulting from 200 μM MO-1 injections (Fig. 7E, F, H, I), or 200 μM MO-trans injections (Fig. 7K, L) and compared to larvae resulting from 200 μM control MO injections (Fig. 7B and C). Although there is some individual variation in the phenotype (Fig. 7, compare D - G, E - H, and F - I), typically there is a reduction in the number of neural fibers and neurons, and an overall disorganization of nerves. The few neural fibers and neurons are present in the brain (Fig. 7F, I, L short arrows) and circumoral nerves (Fig. 7E, F, H, I, K, L double open arrowheads). The main longitudinal connectives in the trunk are visible (Fig. 7E, F, H, I, K, L long arrows), but display various malformations such as axon shortening, pathfinding errors, and presence of a single connective on only one side of the body. In some cases, nerves are severely mispositioned (Fig. 7E, H, K). There is also a lack of commissures and ganglia in the trunk (compare Fig. 7B with E, H and K). The anti-acetylated α-tubulin positive neurons in the head are missing (not shown). The peripheral nervous system is also affected in category III larvae. There is an absence of segmental nerves (Fig. 7E, H, K) and a reduced number of lateral longitudinal nerves in the trunk (Fig. 7E, H, K double open arrows). To gain additional insight into the category III phenotype, one set of 200 μM MO-1 injected larvae was raised for a longer time period and the phenotype examined (6 days instead of 4 days, $n = 201$). Four days after injection, category III larvae (59.7% of total injected ($n = 120/201$)) were separated from the group and observed the following day. Of these, 69.16% ($n = 83/120$) of larvae had elongated but often retained malformations. The remaining 30.83% ($n = 37/120$) had elongated by day 6, but always displayed malformations, such as a bent shape body, absence of visible gut structures and a reduced pygidium. Therefore, 200 μM MO-1 injections resulted in a persistent phenotype that cannot be explained by a simple developmental delay, and there was a lack of recovery of the phenotype when animals were cultured for an extended period. Furthermore, the MO-trans larvae were analyzed five days after microinjection, and the majority of these specimens displayed the same severe category III phenotype.

To summarize, when reduction of *Ct-pax6* was achieved using a splice-blocking morpholino that results in a truncated protein lacking both the paired domain and the paired-type homeodomain, or a translation-blocking morpholino that results in absence of Pax6 protein, the majority of resulting larvae display a strong phenotype, category III, which has a highly reduced number of neurons and neural fibers. Many of the neurons and neural fibers present are disorganized, and are positioned in ectopic locations.

Larvae resulting from injections with 400 μM of MO-2 also show a pronounced nervous system phenotype that sharply contrasts with the normal phenotype (92%, $n = 145/158$) resulting from injections with 400 μM control MO (Fig. 8A, B, C). In larvae injected with 400 μM control MO, segment boundaries and the position of the segmental tissue with respect to the ventral midline is visible (Fig. 8A). Larvae resulting from 400 μM injections of MO-2 predominantly show either a category I or a category II phenotype. First, category I larvae (29%, $n = 66/227$) exhibit a relatively normal gross morphology but exhibit abnormalities in nervous system development (Fig. 8D, E, F). They have visible segment boundaries, although the segmental tissue does not meet at the ventral midline as it normally would at this stage (Fig. 8D). Moreover, category I larvae have a reduced number of segmental nerves (Fig. 8E, unfilled arrowheads), commissures (Fig. 8E, filled arrowheads) and serotonin-positive neurons (Fig. 8F). The observed category II larvae exhibit highly disrupted trunk segmentation with few visible segment boundaries, and the medial edge of the presumptive segmental tissue shows a pronounced lateral displacement (40%, $n = 91/227$; Fig. 8G, H, I). The nervous system of category II larvae appears under-developed. The main longitudinal connectives have thinner neural fibers and are further apart than in control larvae (Fig. 8H and I). In addition, the distance between the nerves from the two contralateral sides increases as one moves posterior, instead of being parallel (Fig. 8H and I). There are few segmental nerves (Fig. 8H, unfilled arrowheads), a reduced number of serotonin-positive neurons in the brain-, circumoral-, and ventral nerve cord region (Fig. 8I), and a lack of commissures (Fig. 8H). Moreover, the lateral longitudinal peripheral nerves are reduced in number in category II larvae (Fig. 8H, double open arrows), but are present in category I larvae (Fig. 8E, double open arrows). The acetylated α-tubulin positive neurons that are typically located anterior to the brain are often altered by *Ct-pax6* transcript reduction (60%, $n = 64/106$). Wildtype larvae possess a bilateral pair with 3 neurons on each side (Fig. 1F and G, asterisks), while larvae resulting from injections with 400 μM MO-2 either have a reduced number of neurons ($n = 39/106$) (Fig. 8E, H, asterisks) or no neurons

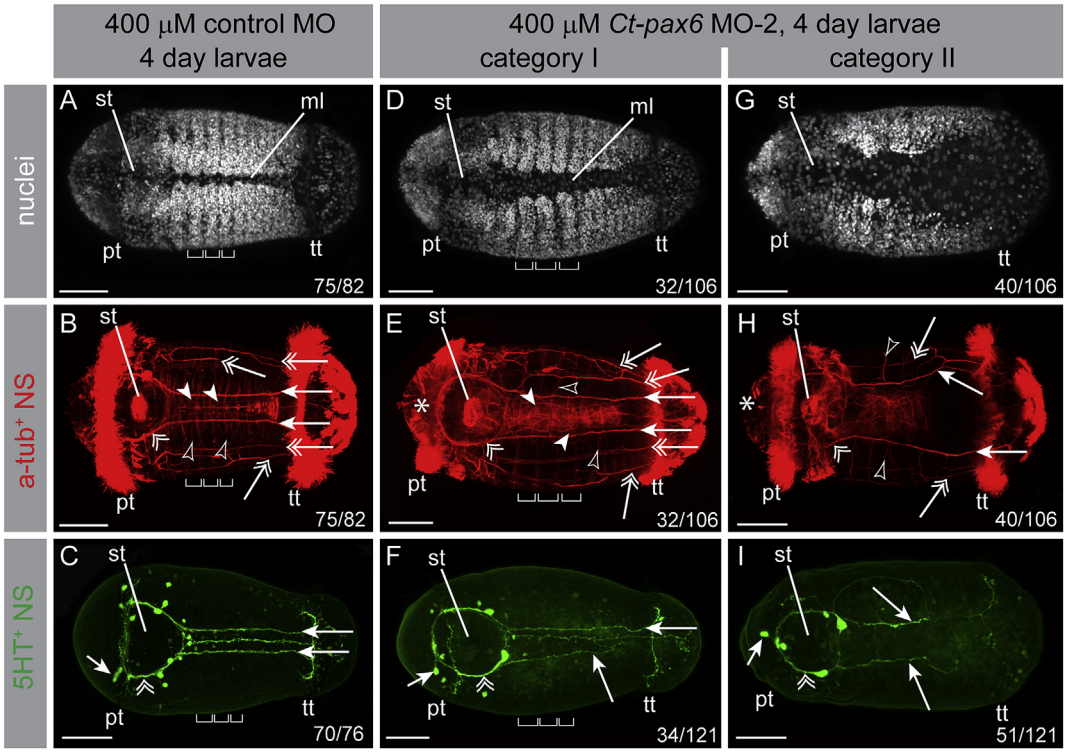

Fig. 8. Nervous system phenotype of *C. teleta* larvae after MO-2 injections. Hoechst staining labels nuclei in white (nuclei; A, D, G), anti-acetylated α-tubulin labeling in red (a-tub^{+} NS; B, E, H) and anti-serotonin labeling in green (5HT^{+} NS; C, F, I). The images in A–B, D–E, and G–H are from the same individual. The developmental time for all larvae shown is four days. All images are z-stack projections, with anterior to the left. Numbers in the right bottom corner indicate the occurrence of the phenotype shown. The brackets in A–F represent the width of individual segments. The double open arrowheads in B, C, E, F, H, and I point towards the circumoral nerves. The main connectives of the ventral nerve cord are indicated by the long arrows in B, C, E, F, H, and I. The commissures in the ventral nerve cord are designated by filled arrowheads in B and E. Unfilled arrowheads highlight selected individual segmental nerves in B, E, and H, while double open arrows point towards the lateral longitudinal nerves. The asterisks in E and H mark the position of the anti-acetylated α-tubulin positive neurons in the head. The short arrows in C, F, and I show the position of serotonin positive neurons in the brain. Abbreviations: ml: ventral midline, pt: prototroch, st: stomodeum, tt: telotroch. Scale bars: 50 µm.

($n = 25/106$). The asymmetric FMRF positive anterior mouth cell (F-AMC), which is located on the left side anterior to the mouth, is altered in 40% ($n = 43/106$) of larvae that result from 400 µM injections of MO-2. This is the only asymmetric, unpaired neuron identified in a previous study (Meyer et al., 2015), and the most common phenotype after *Ct-pax6* knockdown is a loss of this neuron ($n = 38/106$), but occasionally it is present and its position is shifted towards the midline ($n = 5/106$).

To summarize, when a morpholino is used that disrupts splicing of *Ct-pax6* resulting in a truncated protein that contains the paired domain, but does not contain the paired-type homeodomain, most of the resulting larvae show abnormalities in their nervous system. The predominate phenotypes resulting from injections of MO-2 (category I or category II) are considerably less severe than the predominant phenotype resulting from injections of MO-1 injections (category III, Fig. 6).

3.5. Eye phenotype after Ct-pax6 knockdown

Eye development was also analyzed in larvae resulting from *Ct-pax6* MO injections, and microinjection of all three experimental morpholinos exhibited an eye phenotype. The majority of injections of 200 µM of the MO-trans resulted in larvae with no eye pigment (83%, $n = 85/103$). Only a minority of cases have two eyespots (16%, $n = 16/103$), and two specimens have one eyespot (2%, $n = 2/103$). Likewise, larvae resulting from injections with 200 µM MO-1 exhibit a severe eye phenotype when raised for 4 days, and the majority have no eyespots (85%, $n = 226/267$). The remaining cases include larvae with two normal eye pigment spots (9.8%, $n = 26/267$), smaller eyespots (4.5%, $n = 12/267$), and one eyespot (1.1%, $n = 3/267$). Likewise, category II larvae that result from the injection of 400 µM MO-2 also lack pigment ($n = 91/91$). In contrast, the relatively mild phenotype of category I larvae resulting from injections of 400 µM MO-2 allowed for detailed analysis of the eye phenotypes (see below).

The eye phenotype in morphants generated by MO-2 microinjection affect both the pigment cells and the sensory cells present in the eyes of *C. teleta*. The pigment cells and the sensory cells were analyzed independently of each other. The bilateral pair of pigment cells are located dorsally at the lateral-posterior margin of the brain and in close proximity to the prototroch. This pigment cell position is evident in the majority (90%, $n = 143/158$) of larvae resulting from 400 µM control MO injections (Fig. 9A, double open arrowheads). In contrast, only 17% ($n = 41/244$) of category I larvae resulting from injections with 400 µM MO-2 have normal pigment cells. The most prevalent phenotype for most pre MO-2 injected larvae lack pigment cells (40%, $n = 97/244$; Fig. 9B). Additionally, many larvae show abnormal pigment cell formation, such as the presence of only one pigment cell (Fig. 9C; 28%, $n = 68/244$), or a reduction in the size of the pigment cell (Fig. 9D; 16%, $n = 38/244$).

Formation of photo-sensory cells was investigated by reactivity with the 22C10 antibody. Approximately 88% ($n = 67/76$) of larvae resulting from 400 µM control MO injections exhibit the wildtype arrangement of one anterior pair of sensory cells (Fig. 9E, unfilled arrowheads) and one posterior pair of sensory cells (Fig. 9E, filled arrowheads). Similar to the results for pigment cell formation, only a few larvae resulting from injections with 400 µM MO-2 show normal development of sensory cells (8%, $n = 10/121$). There are two predominate sensory cell phenotypes in category I larvae resulting from injections with 400 µM MO-2. The majority of larvae (60%, $n = 73/121$) do not possess any detectable sensory cells (Fig. 9F). Second, a substantial proportion of larvae (31%, $n = 38/$

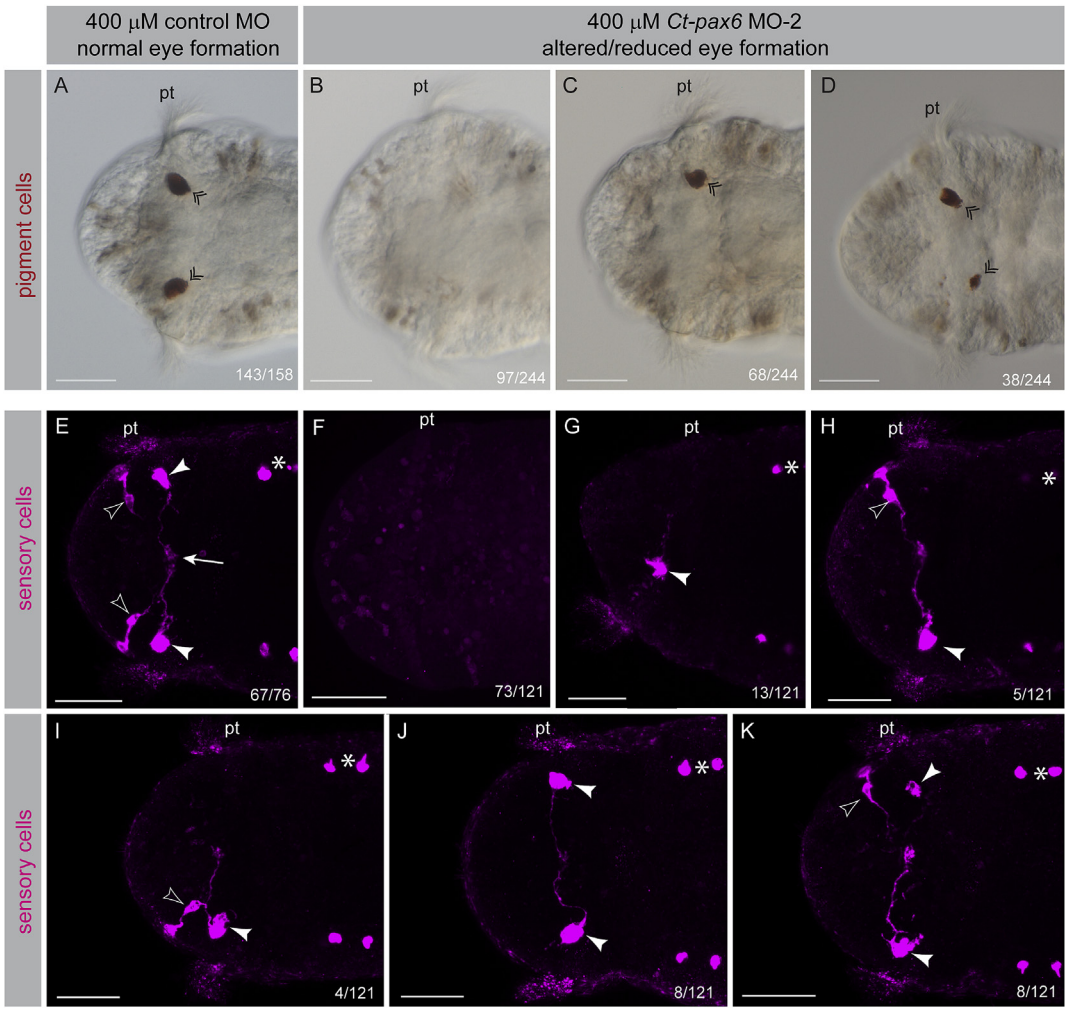

Fig. 9. Eye phenotype of *C. teleta* larvae after MO-2 injections. Brightfield microscopic images to show the eye pigment in dark red (A–D) and 22C10 antibody labeling to label the sensory cells of the eye in magenta (E–K). The developmental time for all larvae shown is four to five days. All images are z-stack projections, with anterior to the left. Numbers in the right bottom corner indicate the occurrence of the phenotype shown. Double open arrowheads in A, C, and D mark the location of the pigment cell. The 22C10 antibody labels four sensory cells: a bilateral anterior pair (E, H, I, K unfilled arrowheads) and a bilateral posterior pair (E, G-K, filled arrowheads). The arrow in E marks the position in the midline of the brain where the axonal projections end. Segmentally iterated chaetae of the trunk are autofluorescent and therefore visible in some of the 22C10 images (asterisks). The posterior sensory cell (filled arrowheads) is associated with the pigment cell (double open arrowheads). Abbreviation: pt: prototroch.

121) have an altered arrangement of sensory cells: presence of one sensory cell (Fig. 9G), presence of one anterior and one posterior sensory cell on different sides of the animal (Fig. 9H), sensory cells on one side of the animal only (Fig. 9I), presence of only anterior or posterior sensory cells on both sides of the head (Fig. 9J), or presence of three sensory cells (Fig. 9K). Both anterior and posterior sensory cells are affected in a similar proportion, which is in line with our finding that *Ct-pax6* is expressed in both cells (see above). To summarize, *Ct-pax6* reduction leads to larvae that either have no eyes or abnormal eye formation. This is evident for both the pigment cells and sensory cells.

3.6. Downstream target analysis of Ct-pax6

Relative expression levels of selected putative target genes were analyzed for larval stages resulting from 400 µM MO-2 injections. Eight genes were selected for preliminary downstream target analysis of Ct-Pax6, and genes were chosen to reflect the observed phenotypes following reduction of *Ct-pax6* transcript, including loss of neural structures and the eye as well as reduced segmentation. First, the effect of Ct-Pax6 on three genes involved in neurogenesis was investigated: *neurogenin* (*Ct-ngn*), *neuroD* (*Ct-neuroD*), and *synaptotagmin 1* (*Ct-syt1*). *Ct-ngn* and *Ct-neuroD* show similar expression patterns during brain and ventral nerve cord neurogenesis in *C. teleta* larvae (Sur et al., 2017), and their temporal and spatial expression often coincides with *Ct-pax6* expression (M. K. personal observation), making both *Ct-ngn* and *Ct-neuroD* potential downstream target genes. *Ct-syt1* is a reliable marker of differentiated, mature neurons in *C. teleta* (Meyer et al., 2015), and its onset appears to be after *Ct-pax6*, which prompted us to investigate the effects of Ct-Pax6 knockdown on *Ct-syt1* expression levels. Second, we examined the effect of Ct-Pax6 on three genes belonging to the gene regulatory network for eye development: *six3/6* (*Ct-six3/6*), *r-opsin* (*Ct-r-opsin1*), and *eyes absent* (*Ct-eya*). Co-expression of *pax6* and *r-opsin* has been demonstrated in the annelid species *P. dumerilii* (Tessmar-Raible et al., 2005). This co-expression is evident in the larval eyes, but not the adult eyes in 72 hpf larvae of *Platynereis*. Moreover, *Ct-r-opsin1* coincides with 22C10 mAb labeling, which marks the photo-sensory cells in *C. teleta* larvae (see Fig. 2), making the gene an ideal target to test whether it is influenced by *Ct-pax6* transcript downregulation. Although there are no expression data for *Ct-six3/6* or *Ct-eya* in *C. teleta*, results from other species suggests that both genes have a conserved role in eye development (Halder et al., 1998; Mannini et al., 2004; Purcell et al., 2005). A third group of genes involved in segment boundary formation were analyzed, since a

disruption of segmentation is a reoccurring phenotype of *Ct-pax6* downregulation (categories II and III). The segmentally iterated expression patterns of *engrailed* (*Ct-en*) (formerly *CapI-en*) (Seaver and Kaneshige, 2006) and a homologue of *lbx/ladybird* (E. C. S. personal observation) makes these genes good candidates for this purpose.

The average fold change values of four biological replicates (one biological replicate represents 150–200 pooled MO injected larvae) are displayed in the bar graph as Fig. 10. All three neurogenesis genes show mild relative transcript level reductions (−0.673, *Ct-neuroD*; −0.798, *Ct-syt1*; −0.939, *Ct-ngn*). A strong reduction of relative transcript levels is evident for the two eye genes *Ct-opsin* (−2.211) and *Ct-eya* (−2.179). Interestingly, *Ct-six3/6*, shows little reduction of relative transcript levels (−0.373). Likewise, there is little down-regulation of the segmentation genes with fold change values of 0.068 for *Ct-lbx* and −0.177 for *Ct-en*. None of these changes are statistically significant when *p* values were calculated using a one-tailed Student's t-test. However, it is noteworthy that *p* values for the two segmentation genes are much higher (around 0.45) than the *p* values of the genes that are known to be *pax6* targets in other species (neurogenesis and eye genes with *p* values between 0.05 and 0.1). Nevertheless, our initial analysis of downstream targets of Ct-Pax6 indicate that in *C. teleta*, Ct-Pax6 may have an inductive effect on *Ct-opsin* and *Ct-eya*, and potentially a mild inductive effect on *Ct-ngn*, *Ct-neuroD*, and *Ct-syt1*.

4. Discussion

The present study represents the first publicly available functional genomic study using morpholino knockdown in *C. teleta*. Here, wildtype transcripts of *Ct-pax6* were reduced in larval stages using two different splice-blocking morpholinos and a translation-blocking morpholino. The results of this study provide evidence that morpholinos are efficient in *C. teleta* and result in specific phenotypes.

4.1. Use of morpholinos to interfere with gene function in Capitella teleta

A number of techniques are now available to study gene function in a wide range of animals. Here, we establish the use of MOs as a targeted method to reproducibly perturb gene function during development in the annelid *C. teleta*. By targeting post-transcriptional stages, MOs act quickly, and therefore provide an important tool for studies of embryonic development. In performing our experiments, we included stringent and widely accepted positive and negative controls (Blum et al., 2015; Eisen and Smith, 2008; Moulton, 2016). Specifically, phenotypes were analyzed from independent microinjections performed with either a splice-blocking or translation-blocking MOs targeted to the single *C. teleta pax6* gene. These MOs are non-overlapping and produce similar phenotypes, demonstrating the specificity of the knockdown phenotype. In animals such as *C. teleta*, splice-blocking MOs offer the advantage of straightforward molecular demonstration of effect and efficiency by RT-qPCR. Microinjections were performed for each MO over a range of concentrations to determine correct dosing and eliminate the possibility of toxicity or off target effects at high concentrations. In future experiments, it is recommended that a range of concentrations be tested for each MO used. A minimum of 3 independent replicates was performed for each MO; a single replicate was defined as injected individuals that developed from a single brood of embryos. The availability of a sequenced genome for *C. teleta* facilitated the design of splice-blocking MOs, and none of the MOs utilized in this study have predicted off targets. The standard control morpholino from GeneTools as well as a 5 bp mismatch morpholino were used, and neither of these morpholinos affects normal development in *C. teleta*. These results demonstrate that morpholino injection into *C. teleta* embryos is not toxic in itself. For the standard MO, a range of concentrations was tested, which will be useful for future experiments. Thus, we have demonstrated specificity of the MOs that target the *pax6* gene and establish guidelines for future functional studies in *C. teleta* by MO knockdown. For developmental studies, the use of MOs to study gene function offers a number of advantages, including the ability to target both maternal and zygotic transcripts simultaneously, study gene function in a tissue-specific manner, target multiple genes at the same time, and study dose depend effects.

Although tools for investigations of gene function during development are more limited in lophotrochozoans than in other clades with well established models, multiple functional techniques are now available, and continue to be developed. Effective use of MOs to generate gene knockdowns has been demonstrated in the leech *H. robusta* (Kuo and Weisblat, 2011), the polychaete *P. dumerilii* (Conzelmann et al., 2013; Williams et al., 2015) and the basket whelk *Tritia* (Chan and Lambert, 2011; Lambert et al., 2016). Targeted mutagenesis in lophotrochozoans was first developed for *P. dumerilii* using TALENs (Bannister et al., 2014), and CRISPR/Cas9-mediated genome modification has been successfully applied to the gastropod molluscs *C. fornicata* and *Lymnaea stagnalis* (Abe and Kuroda, 2019; Perry and Henry, 2015). We also recently established efficient mutagenesis in *C. teleta* using CRISPR/Cas9 genome editing (Neal et al., 2019). Gene knockdown using MOs and targeted mutagenesis using CRISPR/Cas9 are complementary tools (Morcos et al., 2015), and provide exciting new opportunities to address a range of detailed functional questions in *C. teleta*.

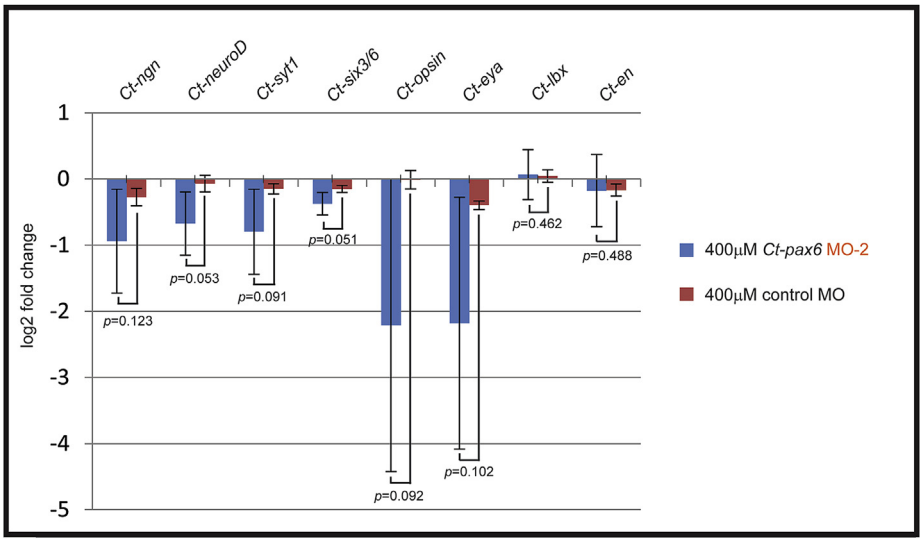

Fig. 10. Relative transcript levels of selected *C. teleta* genes after MO-2 injections. Relative transcript levels after injections of MO-2 (blue) compared to control MO (red). The bar graph shows changes in regulation of transcripts. Error bars (representing standard deviation) as well as corresponding *p*-values are shown (calculated using a one-tailed Student's *t*-test). Note that a logarithmic scale is shown. Abbreviations: *Ct-en*: *C. teleta engrailed*, *Ct-eya*: *C. teleta eyes absent*, *Ct-lbx*: *C. teleta ladybird*, *Ct-ngn*: *C. teleta neurogenin*, *Ct-syt1*: *C. teleta synaptotagmin 1*.

4.2. Evolutionary conservation of pax6

Gene orthology analysis previously identified a single *pax6* orthologue in the *C. teleta* genome that encodes the characteristic highly conserved DNA binding domains, a paired domain and a paired-type homeodomain, as well as a PST-rich transactivation domain (Seaver et al., 2012). The genomic structure of the *Ct-pax6* gene includes ten exons that span over 12 kb. *Pax6* genes from a number of different species are comprised of ten or more exons that occupy a large genomic region: human *pax6* with 14 exons over 22 kb (Glaser et al., 1992; van Heyningen and Williamson, 2002), ascidian *pax6* with 10 exons (Glardon et al., 1997), nematode *pax6* with 14 exons (Chisholm and Horvitz, 1995), and mouse *pax6* with 13 exons (Kleinjan et al., 2004). In *C. teleta*, the paired domain spans two exons, while the paired-type homeodomain is comprised of three exons. Both DNA-binding domains of Pax6 have been implicated in recognizing different downstream targets, and can have divergent roles during development (Ashery-Padan et al., 2000; Chi and Epstein, 2002; Haubst et al., 2004; van Heyningen and Williamson, 2002; Walcher et al., 2013).

4.3. Role of pax6 during eye development

The study of expression and functional involvement of the *pax6* gene during the specification and development of the eye in various species has a long history (Noll, 1993; Cvekl and Callaerts, 2017). Expression of *pax6* associated with developing eyes has been demonstrated in most species investigated and is also found across major phylogenetic lineages: Lophotrochozoa, Ecdysozoa, and Deuterostomia. *C. teleta* belongs to the Annelida, a subclade of the Lophotrochozoa. In *C. teleta Ct-pax6* expression in the larval eye is evident in the sensory cells, but not in the pigment or supporting cells. Association of *pax6* expression with the developing eye has been shown in a few other annelids, including the larval eye of *P. dumerilii* (Arendt et al., 2002), and in the embryo of *Helobdella sp*. (Austin) (Quigley et al., 2007). Representatives of other lophotrochozoan subclades also express *pax6* in association with eye development, such as in squid (Hartmann et al., 2003; Tomarev et al., 1997), cuttlefish (Navet et al., 2009), ribbon worm (Loosli et al., 1996), and plathyhelminthes (Pineda et al., 2002). The ecdysozoan lineage contains many examples where *pax6* expression is found in the developing eye: in the onychophoran *Euperipatoides kanangrensis* (Eriksson et al., 2013), the myriapod *Glomeris marginata* (Prpic, 2005), the wandering spider *Cupiennius salei* (Samadi et al., 2015), the fruit fly *Drosophila melanogaster* (Quiring et al., 1994), and the red flour beetle *Tribolium castaneum* (Yang et al., 2009). There are many chordate representatives showing *pax6* transcripts expressed in the developing eye, including in *Branchiostoma floridae* (Glardon et al., 1998), lamprey (Murakami et al., 2001), lesser spotted dogfish (Ferreiro-Galve et al., 2012), zebrafish (Nornes et al., 1998; Püschel et al., 1992), *Xenopus laevis* (Nakayama et al., 2015), and mouse (Walther and Gruss, 1991). Elaborate eyes are usually comprised of several different cell types and it is noteworthy that *pax6* expression is not necessarily detected in all of them. For example, in the blind Mexican cavefish, *Astyanax mexicanus*, *pax6* expression is reduced in the degenerating lens tissue but remains at normal levels in the retina and ciliary marginal zone (Strickler et al., 2001).

Although there are no functional studies investigating the role of *pax6* during eye development in species closely related to *C. teleta*, the reoccurring expression of *pax6* in the developing eye in a variety of animals (see above) suggests that *pax6* has a functional role in eye formation that is conserved across metazoans. Our *Ct-pax6* knockdown experiments show that normal eye development in *Capitella* larvae is highly impaired in MO injected animals. Interestingly, there is a high correlation between the absence of eyes and severe phenotypic alterations in nervous system development (categories II and III) with all three MOs used in this study. The pronounced eye phenotype in *Capitella* larvae is in accordance with previous studies on a range of species and adds to a substantial body of evidence that the eye specification process relies on functional *pax6*, and is highly conserved across animals. Several individual lines of experimental evidence demonstrate this. First, ectopic expression of *pax6/ey* is sufficient for ectopic eye specification in *Drosophila* (Halder et al., 1995) as well as in *Xenopus* (Chow et al., 1999). Moreover, *pax6* homologues from species as diverse as mouse, ascidian, squid, and cnidarian are capable of inducing ectopic eyes when ectopically expressed in *Drosophila* (Glardon et al., 1997; Halder et al., 1995; Kozmik et al., 2003; Tomarev et al., 1997). Although homozygous *pax6* mutants are typically lethal, heterozygous mutants display varying degrees of eye reduction or malformation, in humans (aniridia disease and Peter's anomaly), mouse, rat, zebrafish, *Xenopus*, and *Drosophila* (Halder et al., 1998; Hill et al., 1991; Kleinjan et al., 2008; Matsuo et al., 1993; Nakayama et al., 2015). Thus, proper *pax6* function is essential for normal eye development in most animals investigated. However, there are some examples where eye development does not involve *pax6* expression, such as in the horseshoe crab (Blackburn et al., 2008).

To further explore the eye phenotype of *Ct-pax6* knockdown in larvae, three genes known to be important during eye development were analyzed using qPCR: *six3/6(optix)*, *r-opsin1*, and *eyes absent(eya)*. In *Drosophila*, *optix/six3/6* is a direct target of Ey/Pax6 (Ostrin et al., 2006), as is its mouse homologue *six3/6* (Purcell et al., 2005), and *six3/6* is predicted to be a Pax6 target in zebrafish (Coutinho et al., 2011). Expression of *six3/6* in the developing eye is widespread among ecdysozoans and deuterostomes (Kumar, 2009b). Direct regulation of *rhodopsin1* by Ey/Pax6 has been demonstrated for *D. melanogaster* (Sheng et al., 1997). It has been confirmed that *eya* is a direct target of Ey/Pax6 in *Drosophila* (Halder et al., 1998; Ostrin et al., 2006) and mouse (Purcell et al., 2005), and *eya* is predicted to be a Pax6 downstream target in zebrafish (Coutinho et al., 2011). Although the result is not statistically significant (due to high biological variability), there is a strong reduction of relative transcript levels for *Ct-opsin* and *Ct-eya* in *Ct-pax6* knockdown larvae. This hints at an evolutionary conservation of *opsin* and *eya* as downstream targets of Pax6. *Ct-six3/6*, however, only shows a minimal reduction of relative transcript levels. Previous studies of *six3/6* function have mainly been conducted in arthropod or vertebrate representatives, where a functional involvement in lens formation has been demonstrated. Many lophotrochozoan eyes do not undergo lens development, which could be a reason why there is no available expression data (Ogura et al., 2013; Pineda and Saló, 2002; Steinmetz et al., 2010).

In summary, our qPCR data suggest that there may be conservation of an eye gene regulatory network that contains *pax6* and *eya* during eye determination, and *opsin* during later stages of eye development. Although further analysis is necessary to explore this in detail, these findings are consistent with the proposed retinal gene network of *D. melanogaster* (Cvekl and Callaerts, 2017; Kumar, 2009a).

4.4. Role of pax6 during nervous system development

A similar expression pattern of *pax6* in the central nervous system during embryonic/larval development is found in all species investigated thus far: typically, expression is in subdomains in the brain and there is an iterative pattern of a subset of cells in the (ventral) nerve cord. Within lophotrochozoans, examples include: planarians (Pineda et al., 2002), leech (Quigley et al., 2007), the annelid *P. dumerilii* (Denes et al., 2007), the ribbon worm (Loosli et al., 1996), and the mollusc *Wirenia argentea* (Scherholz et al., 2017). Within ecdysozoans, examples include *E. kanangrensis* (Eriksson et al., 2013), *Limulus polyphemus* (Blackburn et al., 2008), a myriapod (Prpic, 2005), *T. castaneum* (Yang et al., 2009) and *D. melanogaster* (Quiring et al., 1994), and within chordates the tunicate, *Phallusia mammillata* (Glardon et al., 1997), and the lamprey (Murakami et al., 2001).

In *C. teleta* larvae, initial *Ct-pax6* expression coincides with the onset of the development of the central nervous system. Further maturation of the central nervous system is accompanied by expansion of *Ct-pax6* expression, in distinct subpopulations in the brain and in a segmentally iterative pattern in the ventral nerve cord. This expression pattern of *Ct-*

pax6 transcript suggests that it has at least two roles during neurogenesis. First, it has a role in early neural specification and differentiation, which is represented by the broad expression during larval stages 4–7. Second, *Ct-pax6* has a later role in specifying different neuronal subtypes and/or newly late born neurons, which is represented by the distinct subpopulations of *Ct-pax6* expression. This is in accordance with previous studies that have shown *pax6* to act during different stages of neurogenesis (Blake and Ziman, 2014; Sansom et al., 2009; Shaham et al., 2012). Studies in other animals support the hypothesis that *pax6* has important functions during neuron subtype specification (Aleen Remez et al., 2017; Dulcis et al., 2017; Kroll and O'Leary, 2005; Philips et al., 2005).

Microinjection of either MO-1, MO-2 or MO-trans demonstrates that down-regulation of the wildtype *Ct-pax6* transcript/absence of Ct-Pax6 protein and an increase in incorrectly spliced transcript disrupts normal nervous system development in *C. teleta* larvae. Phenotypic changes include a reduced number of neural fibers and neurons in the brain and the ventral nerve cord. In mouse, it has been shown that Pax6 function is important for neural stem cell renewal (Sansom et al., 2009), and mouse homozygous mutants show a premature cessation of neural progenitor proliferation resulting in fewer neural stem cells present to differentiate into neurons (Philips et al., 2005). This is in line with our MO results, where it appears that fewer neurons are born. Specifically, the knockdown of *Ct-pax6* transcript with both DNA binding motifs missing (MO-1 or MO-trans) results in larvae with a highly reduced number of neurons and neural fibers that form a rudimentary nervous system (anlagen of the brain, circumoral nerves and main longitudinal connectives), resulting in a lack of cells for further maturation. This seems to result in effects on the entire larva. In the trunk, the lack of commissures might be the result of missing ganglionic neurons, since no ganglia have formed. Similarly, zebrafish that were injected with a *pax6b* morpholino or simultaneous injections of *pax6* morpholinos targeting both *pax6* homologues, not only show disrupted eye development, but also a general developmental delay (Kleinjan et al., 2008). In *C. teleta*, along with a decreased number of neurons/neural fibers, there is a general disorganization of neural fibers, which may result from pathfinding defects. For example, the longitudinal connectives are positioned too far apart. These nerves are typically positioned at the margin of the segment anlagen and ventral midline, which might be explained by the presence of pathfinding cues at the margin of the segment anlagen. *Pax6* mutants in *Drosophila* and mouse also show axon pathfinding defects (Jones et al., 2002; Mastick et al., 1997; Noveen et al., 2000), and these phenotypes have been interpreted as being due to defects in axon guidance. Moreover, *ey/pax6 Drosophila* mutants have altered brain morphologies, and display uncoordinated locomotion (Callaerts et al., 2001). Similarly, during murine forebrain development, *pax6* is essential for cell proliferation, fate and patterning as well as for the development of the olfactory system (Haubst et al., 2004; Nomura et al., 2007; Walcher et al., 2013). Thus, *pax6* function is crucial for nervous system development in a range of animals, including in neurogenesis.

To gain further insight into the nervous system phenotype of *Ct-pax6* knockdown larvae, we analyzed three genes involved in neurogenesis via qPCR: *neurogenin* (*Ct-ngn*), *neuroD*, and *synaptotagmin 1* (*Ct-syt1*). Both, *ngn* and *neuroD* are direct targets of Pax6 in mouse and show reduced expression levels in *pax6*-mutant mice (Holm et al., 2007; Sansom et al., 2009; Visel et al., 2007). *SytIV* is predicted to be a direct target of Ey/Pax6 in *D. melanogaster* (Ostrin et al., 2006). Due to variation across biological replicates in our experiments, there is no statistically significant reduction, but nevertheless there is a slight reduction of transcription levels of all three neurogenesis genes in *Ct-pax6* knockdown larvae. Taken together with the observations that these three genes are targets of Pax6 in other species, one might speculate that *ngn*, *neuroD* and *sytIV* are conserved downstream targets of Pax6. Since less attention has been given to the roles of *pax6* during central nervous system development, future functional studies will further unravel its exact functions.

We also analyzed two genes involved in segment boundary formation, *engrailed* and *ladybird*, since disruption of trunk segmentation is a reoccurring phenotype of all three *Ct-pax6* morpholinos. We found that there is no significant downregulation of *Ct-en* or *Ct-lbx*. Nevertheless, Ct-Pax6 has a strong influence on segment boundary formation in *Capitella* larvae, potentially acting through a currently unknown segmentation pathway.

4.5. Conserved functional domains of Pax6 and their roles

To confirm the specificity of the morpholinos to achieve functional knockdown of *Ct-pax6*, a splice-blocking morpholino (MO-1) and a translation-blocking morpholino (MO-trans) were used. These two morpholinos disrupt both the paired domain and homeodomain, and result in very similar severe phenotypes. The observed phenotypes correlate well with the timing of *pax6* expression. Events that occur prior to the onset of *pax6* expression such as global patterning of the body axes are normal. The relationship between the pattern of *pax6* expression and the tissues affected is more complex. In addition to the observed nervous system and eye phenotypes, there is disruption in some tissues that do not express *pax6*. This is most obvious in the lateral ectoderm, where there is a lack of obvious segmentation in the trunk. We propose that there may be a dependency on the nervous system for proper patterning of the trunk ectoderm. Although the mechanism of how this master regulator (*pax6*) influences the development of other tissues is not understood, our results for *C. teleta* are consistent with phenotypes observed in other animals. For example, disruption of the two *pax6* genes in zebrafish leads to a general developmental delay (Kleinjan et al., 2008), and in mouse, homozygous mutants are embryonic lethal (Hill et al., 1991). In addition, mutations in both fly *pax6* homologues (*ey* and *toy*) lead to headless flies (Halder et al., 1998).

A second splice-blocking morpholino (MO-2) was employed, and the two different splice-blocking morpholinos result in larvae with distinct phenotypes. This is expected since the morpholinos were designed to block splicing at different sites in the *pax6* transcript, and hence affect translation of the two conserved DNA binding domains differently. The comparison of the different phenotypes for both splice-blocking MOs suggests that in *C. teleta*, the presence of a paired domain leads to a partial functioning protein since microinjection of MO-2 results in a more mild phenotype. In addition, the paired domain and the paired-type homeodomain of Ct-Pax6 might have different downstream DNA-binding targets, which has been demonstrated for other species (Brandt et al., 2019; Chi and Epstein, 2002; Haubst et al., 2004; van Heyningen and Williamson, 2002; Walcher et al., 2013).

4.6. The homeodomain of Pax6 is involved in eye development

All three MOs used in this study result in larvae with pronounced eye developmental phenotypes. Although a detailed analysis of larvae lacking both functional Pax6 domains (resulting from injection of MO-1 or MO-trans) is difficult due to the phenotypic severity of the resulting larvae, the majority had neither pigment nor sensory cells. If only the DNA binding activities of the paired-type homeodomain is diminished (resulting from injections of MO-2), eye development in the resulting larvae was highly disrupted; ranging from a complete lack of eye cells, a reduction in size, to abnormal development of pigment and sensory cells. Our results are in line with previous studies, which have shown that the paired-type homeodomain of Pax6 is crucial for eye development (Ashery-Padan et al., 2000; van Heyningen and Williamson, 2002). There are a couple of studies of mutants that impair the homeodomain only, for example the original *small eye* mutants in mouse and rat or the hypomorph mouse mutant *Pax64Neu* (Favor et al., 2001; Hill et al., 1991; Matsuo et al., 1993). Typically, homozygous mouse mutants lack eyes and are embryonic lethal, while heterozygous littermates display abnormal eye development including reduction in eye size. Furthermore, Nakayama et al. (2015) showed that targeted mutagenesis in *Xenopus* results in froglets with abnormal eye development when the homeobox of *pax6* is removed. Therefore, mutations in the paired-type homeobox of *pax6* only are sufficient to disrupt normal eye development.

4.7. The paired domain of Pax6 is involved in neurogenesis

The paired domain has been implicated with multiple roles during neurogenesis, such as neuronal subtype specification, axon guidance and neuronal proliferation (Haubst et al., 2004; Huettl et al., 2016; Walcher et al., 2013). However, these effects are variable across species, and suggest that the evolutionary functions of the paired domain are less conserved. Moreover, it has been shown that the paired-type homeodomain is also involved in neuronal regulation, for example in the boundary formation of the mouse brain (Haubst et al., 2004). In *C. teleta*, both DNA binding domains seem to be involved in regulating neurogenesis, since all three morpholinos result in larvae with a reduced number of neurons and neuronal fibers.

4.8. Summary and concluding remarks

Functional studies using splice-blocking and translation-blocking morpholinos in the marine annelid *C. teleta* sufficiently reduce wild-type transcript levels of target genes and are highly reproducible. Transcript expression studies in *C. teleta* larvae and juveniles confirm the presence of *Ct-pax6* in discrete subdomains of the brain and ventral nerve cord as well as in the sensory cells of the larval eye. Reduction of *Ct-pax6* transcript levels results in larvae with both severe eye and nervous system developmental defects. It is notable that from our analysis, we did not identify a simple segregation of function between a role in eye development and a role in neurogenesis between the paired domain and the homeodomain of Pax6 in *C. teleta*. Further studies by targeted disruption of the paired domain, while leaving the paired-type homeodomain intact and analysing larval phenotypes for defects in eye formation and in the nervous system may provide insights into functional differences of these two domains. It has recently been proposed that the ancestral role for *pax6* maybe have been in head patterning and neurogenesis, and that acquiring a role in eye development occurred secondarily (Cvekl and Callaerts, 2017). Taken together, our data supports the concept of an evolutionarily conserved role for *pax6* in the development of both the nervous system and eyes.

Acknowledgements

The authors thank Dr. Danielle de Jong, Alexis Lanza and Leah Dannenberg for helpful suggestions and comments regarding the manuscript, and Alexis Lanza for assistance with confocal imaging of the MO-trans and MO-mismatch specimens. The authors would like to thank Dr. Mansi Srivastava for sharing a protocol on the production of self-made TSA. This work was supported by the National Science Foundation (IOS1457102 to ECS).

Appendix A. Supplementary data

Supplementary data to this article can be found online at https://doi.org/10.1016/j.ydbio.2019.08.011.

References

Abe, M., Kuroda, R., 2019. The development of CRISPR for a mollusc establishes the formin *Lsdia1* as the long-sought gene for snail dextral/sinistral coiling. Development 146 (9). https://doi.org/10.1242/dev.175976.

Aleen Remez, L., Onishi, A., Menuchin-Lasowski, Y., Biran, A., Blackshaw, S., Wahlin, K.J., et al., 2017. Pax6 is essential for the generation of late-born retinal neurons and for inhibition of photoreceptor-fate during late stages of retinogenesis. Dev. Biol. https://doi.org/10.1016/j.ydbio.2017.09.030.

Amiel, A.R., Henry, J.Q., Seaver, E.C., 2013. An organizing activity is required for head patterning and cell fate specification in the polychaete annelid Capitella teleta: new insights into cell-cell signaling in Lophotrochozoa. Dev. Biol. 379 (1), 107–122. https://doi.org/10.1016/j.ydbio.2013.04.011.

Arendt, D., Tessmar, K., de Campos-Baptista, M.I., Dorresteijn, A., Wittbrodt, J., 2002. Development of pigment-cup eyes in the polychaete Platynereis dumerilii and evolutionary conservation of larval eyes in Bilateria. Development 129 (5), 1143–1154.

Ashery-Padan, R., Marquardt, T., Zhou, X., Gruss, P., 2000. Pax6 activity in the lens primordium is required for lens formation and for correct placement of a single retina in the eye. Genes Dev. 14 (21), 2701–2711.

Bannister, S., Antonova, O., Polo, A., Lohs, C., Hallay, N., Valinciute, A., et al., 2014. TALENs mediate efficient and heritable mutation of endogenous genes in the marine annelid Platynereis dumerilii. Genetics 197 (1), 77–89. https://doi.org/10.1534/genetics.113.161091.

Bel-Vialar, S., Medevielle, F., Pituello, F., 2007. The on/off of Pax6 controls the tempo of neuronal differentiation in the developing spinal cord. Dev. Biol. 305 (2), 659–673. https://doi.org/10.1016/j.ydbio.2007.02.012.

Blackburn, D.C., Conley, K.W., Plachetzki, D.C., Kempler, K., Battelle, B.A., Brown, N.L., 2008. Isolation and expression of Pax6 and atonal homologues in the American horseshoe crab, Limulus polyphemus. Dev. Dynam. 237 (8), 2209–2219. https://doi.org/10.1002/dvdy.21634.

Blake, J.A., Ziman, M.R., 2014. Pax genes: regulators of lineage specification and progenitor cell maintenance. Development 141 (4), 737–751. https://doi.org/10.1242/dev.091785.

Blum, M., De Robertis, E.M., Wallingford, J.B., Niehrs, C., 2015. Morpholinos: antisense and sensibility. Dev. Cell 35 (2), 145–149. https://doi.org/10.1016/j.devcel.2015.09.017.

Brandt, J.P., Rossillo, M., Du, Z., Ichikawa, D., Barnes, K., Chen, A., et al., 2019. Lineage context switches the function of a C. elegans Pax6 homolog in determining a neuronal fate. Development 146 (8). https://doi.org/10.1242/dev.168153.

Callaerts, P., Leng, S., Clements, J., Benassayag, C., Cribbs, D., Kang, Y.Y., et al., 2001. Drosophila Pax-6/eyeless is essential for normal adult brain structure and function. J. Neurobiol. 46 (2), 73–88.

Chan, X.Y., Lambert, J.D., 2011. Patterning a spiralian embryo: a segregated RNA for a Tis11 ortholog is required in the 3a and 3b cells of the Ilyanassa embryo. Dev. Biol. 349 (1), 102–112. https://doi.org/10.1016/j.ydbio.2010.10.001.

Chi, N., Epstein, J.A., 2002. Getting your Pax straight: pax proteins in development and disease. Trends Genet. 18 (1), 41–47.

Chisholm, A.D., Horvitz, H.R., 1995. Patterning of the Caenorhabditis elegans head region by the Pax-6 family member vab-3. Nature 377 (6544), 52–55. https://doi.org/10.1038/377052a0.

Chow, R.L., Altmann, C.R., Lang, R.A., Hemmati-Brivanlou, A., 1999. Pax6 induces ectopic eyes in a vertebrate. Development 126 (19), 4213–4222.

Conzelmann, M., Williams, E.A., Tunaru, S., Randel, N., Shahidi, R., Asadulina, A., et al., 2013. Conserved MIP receptor-ligand pair regulates Platynereis larval settlement. Proc. Natl. Acad. Sci. U. S. A. 110 (20), 8224–8229. https://doi.org/10.1073/pnas.1220285110.

Coutinho, P., Pavlou, S., Bhatia, S., Chalmers, K.J., Kleinjan, D.A., van Heyningen, V., 2011. Discovery and assessment of conserved Pax6 target genes and enhancers. Genome Res. 21 (8), 1349–1359. https://doi.org/10.1101/gr.124115.111.

Cvekl, A., Callaerts, P., 2017. PAX6: 25th anniversary and more to learn. Exp. Eye Res. 156, 10–21. https://doi.org/10.1016/j.exer.2016.04.017.

de Jong, D.M., Seaver, E.C., 2016. A stable thoracic hox code and epimorphosis characterize posterior regeneration in Capitella teleta. PLoS One 11 (2), e0149724. https://doi.org/10.1371/journal.pone.0149724.

Denes, A.S., Jékely, G., Steinmetz, P.R., Raible, F., Snyman, H., Prud'homme, B., et al., 2007. Molecular architecture of annelid nerve cord supports common origin of nervous system centralization in bilateria. Cell 129 (2), 277–288. https://doi.org/10.1016/j.cell.2007.02.040.

Dobiasovska, I. (Ed.), 2016. Visual System Development in Platynereis Dumerilii: Insight from Genetic Engineering Approach. (Diploma). Charles University, Prague.

Dulcis, D., Lippi, G., Stark, C.J., Do, L.H., Berg, D.K., Spitzer, N.C., 2017. Neurotransmitter switching regulated by miRNAs controls changes in social preference. Neuron 95 (6), 1319–1333. https://doi.org/10.1016/j.neuron.2017.08.023 e1315.

Eisen, J.S., Smith, J.C., 2008. Controlling morpholino experiments: don't stop making antisense. Development 135 (10), 1735–1743. https://doi.org/10.1242/dev.001115.

Ericson, J., Rashbass, P., Schedl, A., Brenner-Morton, S., Kawakami, A., van Heyningen, V., et al., 1997. Pax6 controls progenitor cell identity and neuronal fate in response to graded Shh signaling. Cell 90 (1), 169–180.

Eriksson, B.J., Samadi, L., Schmid, A., 2013. The expression pattern of the genes engrailed, pax6, otd and six3 with special respect to head and eye development in Euperipatoides kanangrensis Reid 1996 (Onychophora: peripatopsidae). Dev. Gene. Evol. 223 (4), 237–246. https://doi.org/10.1007/s00427-013-0442-z.

Favor, J., Peters, H., Hermann, T., Schmahl, W., Chatterjee, B., Neuhäuser-Klaus, A., Sandulache, R., 2001. Molecular characterization of Pax6(2Neu) through Pax6(10Neu): an extension of the Pax6 allelic series and the identification of two possible hypomorph alleles in the mouse Mus musculus. Genetics 159 (4), 1689–1700.

Ferreiro-Galve, S., Rodríguez-Moldes, I., Candal, E., 2012. Pax6 expression during retinogenesis in sharks: comparison with markers of cell proliferation and neuronal differentiation. J. Exp. Zool. B Mol. Dev. Evol. 318 (2), 91–108. https://doi.org/10.1002/jezb.21448.

Glardon, S., Callaerts, P., Halder, G., Gehring, W.J., 1997. Conservation of Pax-6 in a lower chordate, the ascidian Phallusia mammillata. Development 124 (4), 817–825.

Glardon, S., Holland, L.Z., Gehring, W.J., Holland, N.D., 1998. Isolation and developmental expression of the amphioxus Pax-6 gene (AmphiPax-6): insights into eye and photoreceptor evolution. Development 125 (14), 2701–2710.

Glaser, T., Walton, D.S., Maas, R.L., 1992. Genomic structure, evolutionary conservation and aniridia mutations in the human PAX6 gene. Nat. Genet. 2 (3), 232–239. https://doi.org/10.1038/ng1192-232.

Halder, G., Callaerts, P., Flister, S., Walldorf, U., Kloter, U., Gehring, W.J., 1998. Eyeless initiates the expression of both sine oculis and eyes absent during Drosophila compound eye development. Development 125 (12), 2181–2191.

Halder, G., Callaerts, P., Gehring, W.J., 1995. Induction of ectopic eyes by targeted expression of the eyeless gene in Drosophila. Science 267 (5205), 1788–1792.
Hartmann, B., Lee, P.N., Kang, Y.Y., Tomarev, S., de Couet, H.G., Callaerts, P., 2003. Pax6 in the sepiolid squid Euprymna scolopes: evidence for a role in eye, sensory organ and brain development. Mech. Dev. 120 (2), 177–183.
Haubst, N., Berger, J., Radjendirane, V., Graw, J., Favor, J., Saunders, G.F., et al., 2004. Molecular dissection of Pax6 function: the specific roles of the paired domain and homeodomain in brain development. Development 131 (24), 6131–6140. https://doi.org/10.1242/dev.01524.
Helm, C., Adamo, H., Hourdez, S., Bleidorn, C., 2014. An immunocytochemical window into the development of Platynereis massiliensis (Annelida, Nereididae). Int. J. Dev. Biol. 58 (6–8), 613–622. https://doi.org/10.1387/ijdb.140081cb.
Henry, J.Q., Perry, K.J., Martindale, M.Q., 2010. β-catenin and early development in the gastropod, Crepidula fornicata. Integr. Comp. Biol. 50 (5), 707–719. https://doi.org/10.1093/icb/icq076.
Hill, R.E., Favor, J., Hogan, B.L., Ton, C.C., Saunders, G.F., Hanson, I.M., et al., 1991. Mouse small eye results from mutations in a paired-like homeobox-containing gene. Nature 354 (6354), 522–525. https://doi.org/10.1038/354522a0.
Holm, P.C., Mader, M.T., Haubst, N., Wizenmann, A., Sigvardsson, M., Götz, M., 2007. Loss- and gain-of-function analyses reveal targets of Pax6 in the developing mouse telencephalon. Mol. Cell. Neurosci. 34 (1), 99–119. https://doi.org/10.1016/j.mcn.2006.10.008.
Hopman, A.H., Ramaekers, F.C., Speel, E.J., 1998. Rapid synthesis of biotin-, digoxigenin-, trinitrophenyl-, and fluorochrome-labeled tyramides and their application for in situ hybridization using CARD amplification. J. Histochem. Cytochem. 46 (6), 771–777. https://doi.org/10.1177/002215549804600611.
Huettl, R.E., Eckstein, S., Stahl, T., Petricca, S., Ninkovic, J., Götz, M., Huber, A.B., 2016. Functional dissection of the Pax6 paired domain: roles in neural tube patterning and peripheral nervous system development. Dev. Biol. 413 (1), 86–103. https://doi.org/10.1016/j.ydbio.2015.07.009.
Jones, L., López-Bendito, G., Gruss, P., Stoykova, A., Molnár, Z., 2002. Pax6 is required for the normal development of the forebrain axonal connections. Development 129 (21), 5041–5052.
Jékely, G., Colombelli, J., Hausen, H., Guy, K., Stelzer, E., Nédélec, F., Arendt, D., 2008. Mechanism of phototaxis in marine zooplankton. Nature 456 (7220), 395–399. https://doi.org/10.1038/nature07590.
Kleinjan, D.A., Bancewicz, R.M., Gautier, P., Dahm, R., Schonthaler, H.B., Damante, G., et al., 2008. Subfunctionalization of duplicated zebrafish pax6 genes by cis-regulatory divergence. PLoS Genet. 4 (2), e29. https://doi.org/10.1371/journal.pgen.0040029.
Kleinjan, D.A., Seawright, A., Childs, A.J., van Heyningen, V., 2004. Conserved elements in Pax6 intron 7 involved in (auto)regulation and alternative transcription. Dev. Biol. 265 (2), 462–477.
Kozmik, Z., Daube, M., Frei, E., Norman, B., Kos, L., Dishaw, L.J., et al., 2003. Role of Pax genes in eye evolution: a cnidarian PaxB gene uniting Pax2 and Pax6 functions. Dev. Cell 5 (5), 773–785.
Kroll, T.T., O'Leary, D.D., 2005. Ventralized dorsal telencephalic progenitors in Pax6 mutant mice generate GABA interneurons of a lateral ganglionic eminence fate. Proc. Natl. Acad. Sci. U. S. A. 102 (20), 7374–7379. https://doi.org/10.1073/pnas.0500819102.
Kumar, J.P., 2009a. The molecular circuitry governing retinal determination. Biochim. Biophys. Acta 1789 (4), 306–314. https://doi.org/10.1016/j.bbagrm.2008.10.001.
Kumar, J.P., 2009b. The sine oculis homeobox (SIX) family of transcription factors as regulators of development and disease. Cell. Mol. Life Sci. 66 (4), 565–583. https://doi.org/10.1007/s00018-008-8335-4.
Kuo, D.H., Weisblat, D.A., 2011. A new molecular logic for BMP-mediated dorsoventral patterning in the leech Helobdella. Curr. Biol. 21 (15), 1282–1288. https://doi.org/10.1016/j.cub.2011.06.024.
Lambert, J.D., Johnson, A.B., Hudson, C.N., Chan, A., 2016. Dpp/BMP2-4 mediates signaling from the D-quadrant organizer in a spiralian embryo. Curr. Biol. 26 (15), 2003–2010. https://doi.org/10.1016/j.cub.2016.05.059.
Loosli, F., Kmita-Cunisse, M., Gehring, W.J., 1996. Isolation of a Pax-6 homolog from the ribbonworm Lineus sanguineus. Proc. Natl. Acad. Sci. U. S. A. 93 (7), 2658–2663.
Mannini, L., Rossi, L., Deri, P., Gremigni, V., Salvetti, A., Saló, E., Batistoni, R., 2004. Djeyes absent (Djeya) controls prototypic planarian eye regeneration by cooperating with the transcription factor Djsix-1. Dev. Biol. 269 (2), 346–359. https://doi.org/10.1016/j.ydbio.2004.01.042.
Mansouri, A., Hallonet, M., Gruss, P., 1996. Pax genes and their roles in cell differentiation and development. Curr. Opin. Cell Biol. 8 (6), 851–857.
Mastick, G.S., Davis, N.M., Andrew, G.L., Easter, S.S., 1997. Pax-6 functions in boundary formation and axon guidance in the embryonic mouse forebrain. Development 124 (10), 1985–1997.
Matsunaga, E., Araki, I., Nakamura, H., 2000. Pax6 defines the di-mesencephalic boundary by repressing En1 and Pax2. Development 127 (11), 2357–2365.
Matsuo, T., Osumi-Yamashita, N., Noji, S., Ohuchi, H., Koyama, E., Myokai, F., et al., 1993. A mutation in the Pax-6 gene in rat small eye is associated with impaired migration of midbrain crest cells. Nat. Genet. 3 (4), 299–304. https://doi.org/10.1038/ng0493-299.
Meyer, N.P., Boyle, M.J., Martindale, M.Q., Seaver, E.C., 2010. A comprehensive fate map by intracellular injection of identified blastomeres in the marine polychaete Capitella teleta. EvoDevo 1 (1), 8. https://doi.org/10.1186/2041-9139-1-8.
Meyer, N.P., Carrillo-Baltodano, A., Moore, R.E., Seaver, E.C., 2015. Nervous system development in lecithotrophic larval and juvenile stages of the annelid Capitella teleta. Front. Zool. 12, 15. https://doi.org/10.1186/s12983-015-0108-y.
Morcos, P.A., Vincent, A.C., Moulton, J.D., 2015. Gene editing versus morphants. Zebrafish 12 (5), 319. https://doi.org/10.1089/zeb.2015.1114.
Moulton, J., 2016. Guide for morpholino users: toward therapeutics. J. Drug Discov. Dev. Deliv. 3 (2), 1023.
Murakami, Y., Ogasawara, M., Sugahara, F., Hirano, S., Satoh, N., Kuratani, S., 2001. Identification and expression of the lamprey Pax6 gene: evolutionary origin of the segmented brain of vertebrates. Development 128 (18), 3521–3531.
Nakayama, T., Fisher, M., Nakajima, K., Odeleye, A.O., Zimmerman, K.B., Fish, M.B., et al., 2015. Xenopus pax6 mutants affect eye development and other organ systems, and have phenotypic similarities to human aniridia patients. Dev. Biol. 408 (2), 328–344. https://doi.org/10.1016/j.ydbio.2015.02.012.
Navet, S., Andouche, A., Baratte, S., Bonnaud, L., 2009. Shh and Pax6 have unconventional expression patterns in embryonic morphogenesis in Sepia officinalis (Cephalopoda). Gene Expr. Patterns 9 (7), 461–467. https://doi.org/10.1016/j.gep.2009.08.001.
Neal, S., de Jong, D.M., Seaver, E.C., 2019. CRISPR/CAS9 mutagenesis of a single r-opsin gene blocks phototaxis in a marine larva. Proc Biol Sci 286, 20182491. https://doi.org/10.1098/rspb.2018.2491, 1904.
Noll, M., 1993. Evolution and role of Pax genes. Curr. Opin. Genet. Dev. 3 (4), 595–605.
Nomura, T., Haba, H., Osumi, N., 2007. Role of a transcription factor Pax6 in the developing vertebrate olfactory system. Dev. Growth Differ. 49 (9), 683–690. https://doi.org/10.1111/j.1440-169X.2007.00965.x.
Nornes, S., Clarkson, M., Mikkola, I., Pedersen, M., Bardsley, A., Martinez, J.P., et al., 1998. Zebrafish contains two pax6 genes involved in eye development. Mech. Dev. 77 (2), 185–196.
Noveen, A., Daniel, A., Hartenstein, V., 2000. Early development of the Drosophila mushroom body: the roles of eyeless and dachshund. Development 127 (16), 3475–3488.
Ogura, A., Yoshida, M.A., Moritaki, T., Okuda, Y., Sese, J., Shimizu, K.K., et al., 2013. Loss of the six3/6 controlling pathways might have resulted in pinhole-eye evolution in Nautilus. Sci. Rep. 3, 1432. https://doi.org/10.1038/srep01432.
Ostrin, E.J., Li, Y., Hoffman, K., Liu, J., Wang, K., Zhang, L., et al., 2006. Genome-wide identification of direct targets of the Drosophila retinal determination protein Eyeless. Genome Res. 16 (4), 466–476. https://doi.org/10.1101/gr.4673006.
Pechenik, J.A., Berard, R., Kerr, L., 2000. Effects of reduced salinity on survival, growth, reproductive success, and energetics of the euryhaline polychaete Capitella sp. I. J. Exp. Mar. Biol. Ecol. 254 (1), 19–35.
Pechenik, J.A., Chaparro, O.R., Pilnick, A., Karp, M., Acquafredda, M., Burns, R., 2016. Effects of embryonic exposure to salinity stress or hypoxia on post-metamorphic growth and survival of the polychaete Capitella teleta. Biol. Bull. 231 (2), 103–112. https://doi.org/10.1086/690090.
Perry, K.J., Henry, J.Q., 2015. CRISPR/Cas9-mediated genome modification in the mollusc, Crepidula fornicata. Genesis 53 (2), 237–244. https://doi.org/10.1002/dvg.22843.
Pfaffl, M.W., 2001. A new mathematical model for relative quantification in real-time RT-PCR. Nucleic Acids Res. 29 (9), e45.
Philips, G.T., Stair, C.N., Young Lee, H., Wroblewski, E., Berberoglu, M.A., Brown, N.L., Mastick, G.S., 2005. Precocious retinal neurons: pax6 controls timing of differentiation and determination of cell type. Dev. Biol. 279 (2), 308–321. https://doi.org/10.1016/j.ydbio.2004.12.018.
Pineda, D., Rossi, L., Batistoni, R., Salvetti, A., Marsal, M., Gremigni, V., et al., 2002. The genetic network of prototypic planarian eye regeneration is Pax6 independent. Development 129 (6), 1423–1434.
Pineda, D., Saló, E., 2002. Planarian Gtsix3, a member of the Six/so gene family, is expressed in brain branches but not in eye cells. Mech. Dev. 119 (Suppl. 1), S167–S171.
Prpic, N.M., 2005. Duplicated Pax6 genes in Glomeris marginata (Myriapoda: diplopoda), an arthropod with simple lateral eyes. Zoology (Jena) 108 (1), 47–53. https://doi.org/10.1016/j.zool.2004.11.003.
Purcell, P., Oliver, G., Mardon, G., Donner, A.L., Maas, R.L., 2005. Pax6-dependence of Six3, Eya1 and Dach1 expression during lens and nasal placode induction. Gene Expr. Patterns 6 (1), 110–118. https://doi.org/10.1016/j.modgep.2005.04.010.
Püschel, A.W., Gruss, P., Westerfield, M., 1992. Sequence and expression pattern of pax-6 are highly conserved between zebrafish and mice. Development 114 (3), 643–651.
Quigley, I.K., Xie, X., Shankland, M., 2007. Hau-Pax6A expression in the central nervous system of the leech embryo. Dev. Gene. Evol. 217 (6), 459–468. https://doi.org/10.1007/s00427-007-0156-1.
Quiring, R., Walldorf, U., Kloter, U., Gehring, W.J., 1994. Homology of the eyeless gene of Drosophila to the Small eye gene in mice and Aniridia in humans. Science 265 (5173), 785–789.
Rabinowitz, J.S., Chan, X.Y., Kingsley, E.P., Duan, Y., Lambert, J.D., 2008. Nanos is required in somatic blast cell lineages in the posterior of a mollusk embryo. Curr. Biol. 18 (5), 331–336. https://doi.org/10.1016/j.cub.2008.01.055.
Ravi, V., Bhatia, S., Gautier, P., Loosli, F., Tay, B.H., Tay, A., et al., 2013. Sequencing of Pax6 loci from the elephant shark reveals a family of Pax6 genes in vertebrate genomes, forged by ancient duplications and divergences. PLoS Genet. 9 (1), e1003177. https://doi.org/10.1371/journal.pgen.1003177.
Rhode, B., 1993. Larval and adult eyes in *Capitella spec. I* (Annelida, Polychaeta)Larval and adult eyes in Capitella spec. I (Annelida, Polychaeta). J. Morphol. 217 (3), 327–335. https://doi.org/10.1002/jmor.1052170307.
Samadi, L., Schmid, A., Eriksson, B.J., 2015. Differential expression of retinal determination genes in the principal and secondary eyes of Cupiennius salei Keyserling (1877). EvoDevo 6, 16. https://doi.org/10.1186/s13227-015-0010-x.
Sansom, S.N., Griffiths, D.S., Faedo, A., Kleinjan, D.J., Ruan, Y., Smith, J., et al., 2009. The level of the transcription factor Pax6 is essential for controlling the balance between neural stem cell self-renewal and neurogenesis. PLoS Genet. 5 (6), e1000511. https://doi.org/10.1371/journal.pgen.1000511.

Scardigli, R., Bäumer, N., Gruss, P., Guillemot, F., Le Roux, I., 2003. Direct and concentration-dependent regulation of the proneural gene Neurogenin2 by Pax6. Development 130 (14), 3269–3281.

Scherholz, M., Redl, E., Wollesen, T., de Oliveira, A.L., Todt, C., Wanninger, A., 2017. Ancestral and novel roles of Pax family genes in mollusks. BMC Evol. Biol. 17 (1), 81. https://doi.org/10.1186/s12862-017-0919-x.

Seaver, E.C., 2016. Annelid models I: Capitella teleta. Curr. Opin. Genet. Dev. 39, 35–41. https://doi.org/10.1016/j.gde.2016.05.025.

Seaver, E.C., Kaneshige, L.M., 2006. Expression of 'segmentation' genes during larval and juvenile development in the polychaetes Capitella sp. I and H. elegans. Dev. Biol. 289 (1), 179–194. https://doi.org/10.1016/j.ydbio.2005.10.025.

Seaver, E.C., Paulson, D.A., Irvine, S.Q., Martindale, M.Q., 2001. The spatial and temporal expression of Ch-en, the engrailed gene in the polychaete Chaetopterus, does not support a role in body axis segmentation. Dev. Biol. 236 (1), 195–209. https://doi.org/10.1006/dbio.2001.0309.

Seaver, E.C., Thamm, K., Hill, S.D., 2005. Growth patterns during segmentation in the two polychaete annelids, Capitella sp. I and Hydroides elegans: comparisons at distinct life history stages. Evol. Dev. 7 (4), 312–326. https://doi.org/10.1111/j.1525-142X.2005.05037.x.

Seaver, E.C., Yamaguchi, E., Richards, G.S., Meyer, N.P., 2012. Expression of the pair-rule gene homologs runt, Pax3/7, even-skipped-1 and even-skipped-2 during larval and juvenile development of the polychaete annelid Capitella teleta does not support a role in segmentation. EvoDevo 3, 8. https://doi.org/10.1186/2041-9139-3-8.

Shaham, O., Menuchin, Y., Farhy, C., Ashery-Padan, R., 2012. Pax6: a multi-level regulator of ocular development. Prog. Retin. Eye Res. 31 (5), 351–376. https://doi.org/10.1016/j.preteyeres.2012.04.002.

Sheng, G., Thouvenot, E., Schmucker, D., Wilson, D.S., Desplan, C., 1997. Direct regulation of rhodopsin 1 by Pax-6/eyeless in Drosophila: evidence for a conserved function in photoreceptors. Genes Dev. 11 (9), 1122–1131.

Song, M.H., Huang, F.Z., Chang, G.Y., Weisblat, D.A., 2002. Expression and function of an even-skipped homolog in the leech Helobdella robusta. Development 129 (15), 3681–3692.

Steinmetz, P.R., Urbach, R., Posnien, N., Eriksson, J., Kostyuchenko, R.P., Brena, C., et al., 2010. Six3 demarcates the anterior-most developing brain region in bilaterian animals. EvoDevo 1 (1), 14. https://doi.org/10.1186/2041-9139-1-14.

Strickler, A.G., Yamamoto, Y., Jeffery, W.R., 2001. Early and late changes in Pax6 expression accompany eye degeneration during cavefish development. Dev. Gene. Evol. 211 (3), 138–144.

Sur, A., Magie, C.R., Seaver, E.C., Meyer, N.P., 2017. Spatiotemporal regulation of nervous system development in the annelid Capitella teleta. EvoDevo 8, 13. https://doi.org/10.1186/s13227-017-0076-8.

Tessmar-Raible, K., Steinmetz, P.R., Snyman, H., Hassel, M., Arendt, D., 2005. Fluorescent two-color whole mount in situ hybridization in Platynereis dumerilii (Polychaeta, Annelida), an emerging marine molecular model for evolution and development. Biotechniques 39 (4), 460, 462, 464.

Tomarev, S.I., Callaerts, P., Kos, L., Zinovieva, R., Halder, G., Gehring, W., Piatigorsky, J., 1997. Squid Pax-6 and eye development. Proc. Natl. Acad. Sci. U. S. A. 94 (6), 2421–2426.

van Heyningen, V., Williamson, K.A., 2002. PAX6 in sensory development. Hum. Mol. Genet. 11 (10), 1161–1167.

Visel, A., Carson, J., Oldekamp, J., Warnecke, M., Jakubcakova, V., Zhou, X., et al., 2007. Regulatory pathway analysis by high-throughput in situ hybridization. PLoS Genet. 3 (10), 1867–1883. https://doi.org/10.1371/journal.pgen.0030178.

Walcher, T., Xie, Q., Sun, J., Irmler, M., Beckers, J., Öztürk, T., et al., 2013. Functional dissection of the paired domain of Pax6 reveals molecular mechanisms of coordinating neurogenesis and proliferation. Development 140 (5), 1123–1136. https://doi.org/10.1242/dev.082875.

Walther, C., Gruss, P., 1991. Pax-6, a murine paired box gene, is expressed in the developing CNS. Development 113 (4), 1435–1449.

Williams, E.A., Conzelmann, M., Jékely, G., 2015. Myoinhibitory peptide regulates feeding in the marine annelid Platynereis. Front. Zool. 12 (1), 1. https://doi.org/10.1186/s12983-014-0093-6.

Yamaguchi, E., Seaver, E.C., 2013. The importance of larval eyes in the polychaete *Capitella teleta*: effects of larval eye deletion on formation of the adult eyesThe importance of larval eyes in the polychaete Capitella teleta: effects of larval eye deletion on formation of the adult eyes. Invertebr. Biol. 132 (4), 352–367. https://doi.org/10.1111/ivb.12034.

Yang, X., Weber, M., Zarinkamar, N., Posnien, N., Friedrich, F., Wigand, B., et al., 2009. Probing the Drosophila retinal determination gene network in Tribolium (II): the Pax6 genes eyeless and twin of eyeless. Dev. Biol. 333 (1), 215–227. https://doi.org/10.1016/j.ydbio.2009.06.013.

Zwarycz, A.S., Nossa, C.W., Putnam, N.H., Ryan, J.F., 2015. Timing and scope of genomic expansion within Annelida: evidence from homeoboxes in the genome of the earthworm Eisenia fetida. Genome Biol Evol 8 (1), 271–281. https://doi.org/10.1093/gbe/evv243.